

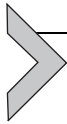
**Provided for non-commercial research and educational use only.
Not for reproduction, distribution or commercial use.**

This chapter was originally published in the book *Advances in Heat Transfer, Vol. 45*, published by Elsevier, and the attached copy is provided by Elsevier for the author's benefit and for the benefit of the author's institution, for non-commercial research and educational use including without limitation use in instruction at your institution, sending it to specific colleagues who know you, and providing a copy to your institution's administrator.



All other uses, reproduction and distribution, including without limitation commercial reprints, selling or licensing copies or access, or posting on open internet sites, your personal or institution's website or repository, are prohibited. For exceptions, permission may be sought for such use through Elsevier's permissions site at: <http://www.elsevier.com/locate/permissionusematerial>

From: Brian Spalding, Trends, Tricks, and Try-ons in CFD/CHT.
In Ephraim M. Sparrow, Young I. Cho, John P. Abraham and
John M. Gorman, editors: *Advances in Heat Transfer, Vol. 45*,
Burlington: Academic Press, 2013, pp. 1-78.
ISBN: 978-0-12-407819-2
© Copyright 2013 Elsevier Inc.
Academic Press



Trends, Tricks, and Try-ons in CFD/CHT

Brian Spalding

CHAM Ltd, 40 High St Wimbledon, London SW 19 5AU, United Kingdom

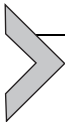
Contents

1. Introduction	2
2. Trends	2
2.1 Computational grid trends	2
2.2 Linear equation solver trends	9
2.3 Turbulence model trends	16
3. Tricks	35
3.1 The IMMERSOL radiation model	35
3.2 The wall-distance trick	43
3.3 The cut-link trick	48
4. Try-ons	61
4.1 A differential equation for mixing length	61
4.2 The population approach to swirling flow	65
4.3 Hybrid CFD "Try-on"	67
5. Concluding Remarks	75
References	75

Abstract

Computational fluid dynamics and its counterpart computational heat transfer are subjects that inspire alarm in precomputer-trained professors and awe in young would-be researchers. One aim of this chapter is to diminish these reactions by clarifying both the laudable and the debatable natures of the subjects. A second aim is to make clear, to those who are not overanxious to follow fashion, that there remains much scope for valuable innovations.

The chapter reviews items selected from approximately half a century of three-steps-forward-two-steps-back actions, and it contains such adumbrations of detail and expressions of personal opinion as its author judges to be conducive to its aim.



1. INTRODUCTION

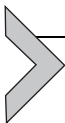
Science, whether pure or applied, is no less subject to fashion than other human activities. Following one's predecessors is usually safe and sometimes wise; but it is best done consciously, with the possibility in mind that *not* following may sometimes be better.

The “trends” referred to in the title of the chapter can be fairly called “fashions.” Examples will be discussed in respect to computational grids, equation-solving methods, and turbulence models.

Reality *is* and theory *may* be, but it is the latter that scientists prefer to deal with. Just as the theater “magician” persuades his audience to believe in what can surely not be truth, so the inventive scientist seeks to persuade himself, and indeed others too, that his idealizations, though not strictly true, will be *useful*. Lest they be overprotected from criticisms, such artifacts are here called “tricks.” Radiation models and techniques for handling awkwardly shaped objects are among the contributions of the computational fluid dynamics/computational heat transfer (CFD/CHT) “tricksters.”

Before a novel approach becomes an accepted trick and is honored with the grander title of “model,” it appears as a “try-on,” by which is here meant that its proposer “wonders if” some new formulation might possibly fit reality better than those in common use. Examples of such musings, in which the author will invite his readers to participate, concern a “mixing length transport” turbulence model, the “population model” approach to turbulent swirling flows, and the “partially parabolic” method.

During the writing of this chapter, the author has been conscious of the serious gaps in his own current knowledge, by exposing which he hopes that some readers will be moved to enlighten him. Should his ignorance prove to be widely shared, however, exposing it may hopefully guide researchers toward avenues that may be profitable to explore.



2. TRENDS

2.1. Computational grid trends

2.1.1 *Early choices: Cartesian, cylindrical-polar, and body-fitted*

The earliest applications of numerical solution methods to the differential equations of fluid mechanics and heat transfer used grids of Cartesian or cylindrical-polar configuration. Formulating the so-called finite-difference (later “finite-volume”) equations linking dependent variables at grid nodes

was then rather easy because lines joining such nodes intersected at right angles. Typically, each node was connected with only six neighbors, two in each of the three coordinate directions.

Soon, however, the need to consider flows around curved bodies such as airfoils caused “*body-fitted coordinate*” grids to find favor, even though at least 12 neighbors had to be considered for each node; and still, the equations could be formulated plausibly in more than one way.

2.1.2 *Arbitrary polygonal cells*

Specialists in the analysis of stresses in solids had meanwhile been taking a different route. Their “finite volumes,” which they called “finite elements,” were typically tetrahedrons with arbitrary angles between the normal and adjacent sides. This choice allowed their grids to be fitted to bodies of rather awkward shapes, which was probably the reason why fluid dynamicists also began to adopt the idea.

The equations between the variables at the grid nodes now became even more complex and difficult to derive with certainty; but, once done and embodied in computer coding, the difficulties disappeared from view. Reluctance to revisit them discouraged making rigorous tests as to the relative accuracies of the alternative discretization possibilities. (Question #1 to readers: where, if anywhere, have the results of truly comprehensive tests been published?)

Grids of this kind were “unstructured,” meaning that geometrically nearby nodes did not necessarily have their values stored in adjacent locations in computer memory. This complicated the task of solving the equations; and for this reason, some computer-code custodians preferred not to follow the fashion, adopting instead a different way of solving the awkward-body-shape problem. They used the “cut-cell” technique.

2.1.3 *PARSOL: for “partly solid” cells*

In one version of this technique, known as PARSOL [58], the grid was everywhere of the structured Cartesian or cylindrical-polar configuration *except* where cell edges were intersected by the surfaces of solid bodies. Cells having such intersected edges were then split into two parts, one within the body and one outside it. Moreover, this was performed automatically by the computer code; so the bothersome-to-users task of creating an unstructured grid ceased to exist.

Figure 1.1 shows an early example of the application of this technique to the flow of air through a louvered wall. Of course, the Cartesian grid had to

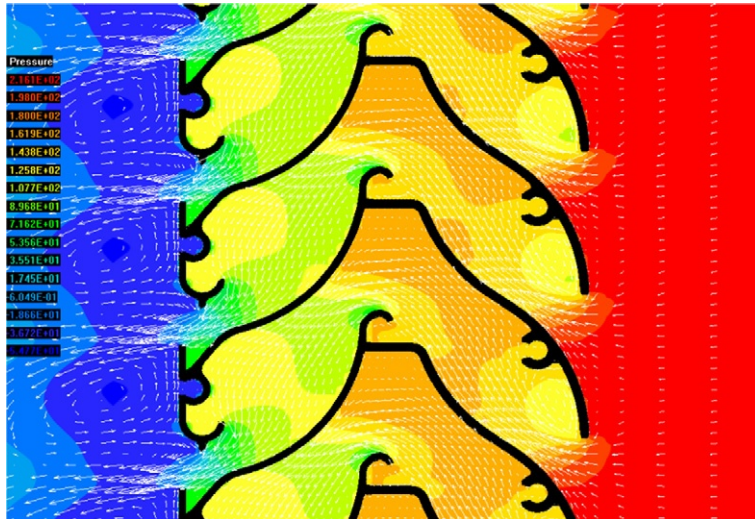


Figure 1.1 PARSOL applied to a louver.

be fine enough so that no cell had *two* nonsolid parts in it; but it could not be so fine as properly to represent the boundary layers on the louver surfaces.

2.1.4 Space-averaged rather than detailed-geometry CFD

Early in the present author's career, he had to apply CFD to practical problems in which the detailed geometry of the equipment in question was too intricate to be fitted by any grid that had a cell number small enough for the then-available computers to handle. Specifically, it was necessary to be able, at least to some extent, to simulate the flow of mixtures of steam and water through spaces between the hot water-containing tubes within the shells of nuclear steam generators [1].

Both body-fitted and cut-cell grids were out of the question, because the dimensions of the largest possible grids greatly exceeded tube diameters. Therefore, the heat transfer and frictional interactions between the fluid mixture and the tube bundle were represented via "space averaging." This entailed postulating that coefficients having per-unit-volume dimensions would be able sufficiently to represent the interactions quantitatively; and their local magnitudes were either guessed or computed from believed-to-be plausible formulas. From them were computed the magnitudes per unit shell volume of the heat sinks within the tube-side water and the heat sources in the shell-side mixture.

This was one of the first of the “tricks” alluded to in the title of this chapter. It was accepted as the best that could be done; and it helped steam-generator designers to reduce the flow-induced damage that was then limiting the life spans of their equipment.

2.1.5 IBM: the immersed boundary method

Tube bundles were treated by space-averaged CFD as being “immersed” in the fluids within and outside them. It is interesting therefore that what is called the “immersed boundary method” is becoming popular [2] as a means of avoiding the unstructured grid-creation difficulty. The essential idea is similar to that of space-averaged CFD. It adds such sources or sinks to the finite-volume momentum equations as will reduce to zero the velocities at locations *within* the solid and such as will also ensure that the velocity components at points *just outside* the solid produce vectors parallel to its surface.

As with PARSOL, the grid must be fine enough, when the solid body is thin, for the grid nodes to represent its shape adequately; and the magnitudes of the sources can be computed with various degrees of sophistication. However, the simplicity of the method is such that former enthusiasts for the polygonal cell shape policy appear to be transferring their affections.

Although only now becoming fashionable, its acknowledged roots are old [59]. Figure 1.2 shows a 1995 application to the simulation of air flow within a football stadium [3].

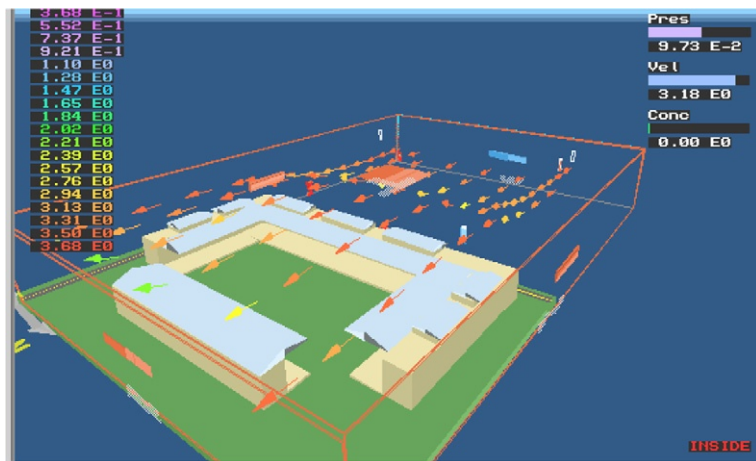


Figure 1.2 Early example of immersed boundary technique.

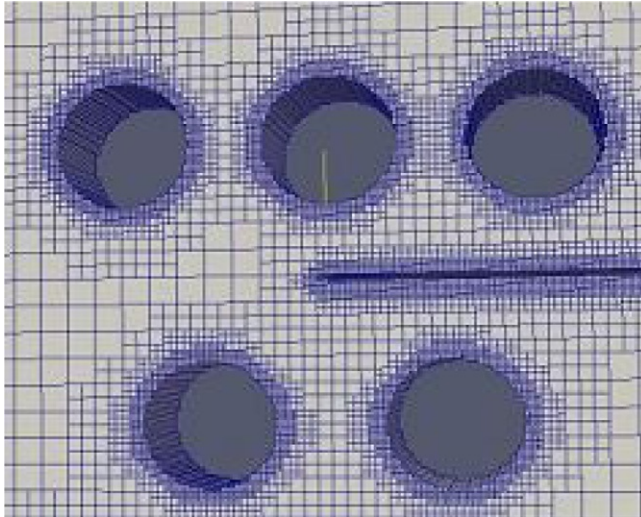


Figure 1.3 Divided Cartesian grid.

2.1.6 Divided Cartesian grids

It must be admitted that the polygonal cell shape policy does allow the grid to be fine only close to solid surfaces while remaining coarser elsewhere. For this reason, some CFD-code vendors have adopted a compromise solution of the kind illustrated in Fig. 1.3, in which the larger still-Cartesian cells are successively halved in one or all directions, with the smallest cells being closest to the solid surfaces where they are most needed.

To judge from recent CFD publications [60], such grids are becoming more popular than arbitrary polygonal ones, no doubt because the finite-volume equations are easier to formulate.

2.1.7 The future

Body-fitted, cut-cell, immersed boundary, and subdivided grids all have their distinct merits; moreover, they are not incompatible with one another. The present author is therefore working on creating grids that combine all features, seeing in such a combination the best that can be envisaged at the present time. The once ubiquitous arbitrary polygonal grid, however, seems unlikely to retain its popularity.

Some success has been obtained with what has been called the X-cell grid, a simple version of which is shown in Fig. 1.4. An interesting feature

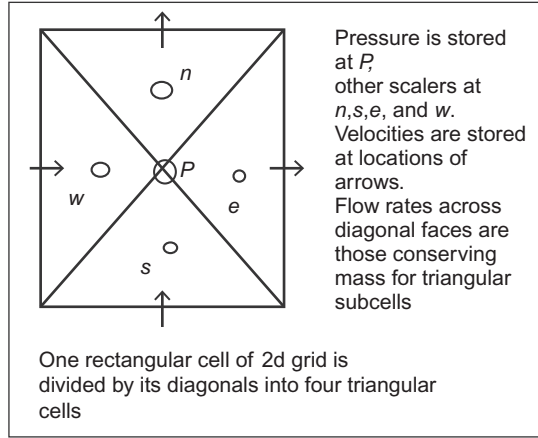


Figure 1.4 The X-cell grid.

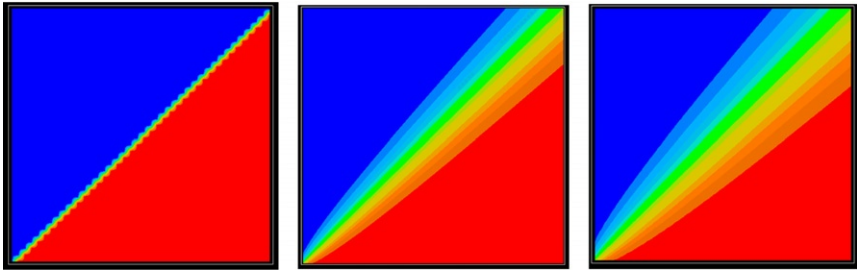


Figure 1.5 Showing the superior numerical-diffusion suppression of X-cells.

of this grid type is that the number of control volumes provided for scalar variables such as temperature is four times the numbers of control volumes for mass and momentum conservation. This is not unreasonable because distributions of pressure within fluids, which are deduced from the latter equations, are commonly much more smooth than those of temperature.

More important however than the increase in number is their difference in *shape*; whereas rectangular cells are free from numerical diffusion only when the fluid flows *vertically* or horizontally, X-cell grids are free from it for *diagonally directed* flow. This is illustrated in the three contour diagrams of Fig. 1.5. All of these represent the predicted temperature distribution in a two-dimensional (2D) equal-sided domain, into which colder (blue) fluid flows from the left and hotter (red) fluid flows, with equal absolute velocity, from below. The grid is uniform with 40 rows and 40 columns in diagrams (a) and (b), but it has 80 rows and 80 columns in diagram (c).

The cells of (a) are divided in the X-cell manner; and, as a consequence, the temperature-discontinuity boundary between the two streams remains perfectly sharp. Those of (b) and (c) are not so divided; therefore, the numerical diffusion associated with the conventional upwind differencing causes the interface to become blurred. The blurring is less for case (c), which has the same number of control volumes as case (a); but it is still severe. It is the *triangular shape* of the extra control volumes of X-cell that makes the difference, not their number.

Figure 1.5 admittedly shows X-cell at its spectacularly successful best, because the flow direction is aligned with one of the diagonals. But X-cell is better than the conventional grid of the same number of control volumes *whatever* the flow direction.

Some work has been done on a more advanced version of X-cell in which the velocity components are stored at the same locations as the scalar variables. This gives the grid a so-called collocated character, which has the advantage that the convective contributions to the internode coefficients are the same for both all dependent variables. But there is another advantage too: The pressures are *not* stored at the same location; therefore, the “checker-board problem” associated with the usual collocated-grid arrangement does not arise!

Attractive though it is, lack of publicity has left this possibility scarcely explored. All that can be reported is that the present author with S. Zhubrin [Ref. 57], several years ago, compared the results of such X-cell-based calculations with results obtained with a body-fitted coordinate grid having an equal number of cells. The flow was the 2D steady laminar flow around and in the wake of a cylinder positioned at right angles to the stream. A comparison of the numerical predictions of the nondimensionalized length of the downstream recirculation zone with the experimental value is conveyed in Table 1.1.

While insufficient in number to be conclusive, these comparisons suggest that X-cell is greatly superior when the grid is coarse.

Table 1.1 Comparison of Numerical Predictions and Experimental Data for Wake Length

$NX * NY$	Length 1; X-cell	Length 2; BFC	Length 3; exprm
$27 * 13$	2.3	1.15	2.75
$36 * 13$	2.6	1.25	2.75
$60 * 30$	2.8	2.8	2.75

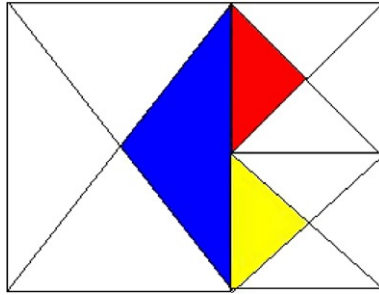


Figure 1.6 X-cell subdivision combined with Cartesian subdivision.

The purpose of this chapter is more to point out possibilities than to enumerate certainties. It is therefore appropriate to remark that the X-cell idea is applicable to unstructured Cartesian grids and to structured ones. [Figure 1.6](#) explains clearly enough.

Of course, there is no need to use X-cell subdivision everywhere. For reasons of economy, it would make sense to use it only, so as to preserve realism, where numerical diffusion would otherwise outweigh physical diffusion.

The subject of computational grids will be returned to under “Tricks” in [Section 3.3](#).

2.2. Linear equation solver trends

2.2.1 *Point-by-point (i.e., PBP) relaxation methods*

Although the presence of convection terms in the finite-volume equations of CFD renders their totality *nonlinear*, it is common practice to proceed by way of solving a series of equations for a *single dependent* variable. These equations are treated as being temporarily *linear*, by updating their coefficients in what are called “outer iterations,” only after all such variables have been attended to.

Parenthetically, it may be remarked that whether this is wise is still doubted by those who remember the SIVA (i.e., simultaneous variable adjustment) method of the early 1970s [4]. It was doing well before it was swept aside by the incursion of SIMPLE (i.e., semi-implicit method for pressure-linked equations) [5]; and surely, SIVA could have been further improved. But decade-long eclipses like this are frequent consequences of science’s fashion-following tendency.

The form of the linear equations to be solved is

$$a_{ii}x_i + \sum_j a_{ij}x_j = b_i$$

where x_i is the value of a dependent variable at node i , x_j is its value at the neighboring nodes j , a_{ii} , and a_{ij} are constant coefficients, and b_i is a source term.

These equations may easily be solved, point-by-point, by updating each x_i in turn, while the x_j 's on the right-hand side are treated temporarily as known values, until, that is, they are updated when their turn comes round. Then, as soon as the last value has been updated, a new cycle of updates can be undertaken, so as to determine what adjustments of the first-made updates must be made to accord with the later-made ones.

The updating process just described is often (but not always) called "relaxation." That term will be used in the succeeding text.

The two most common PBP relaxation methods are

- Gauss–Seidel that uses the updated x_j 's as soon as they are available and
 - Jacobi that delays the updating until each node has been visited once.
- The former converges toward the solution more rapidly; but both require many repeated relaxations; and their number increases in proportion to the square or higher power of the number of nodes in the grid.

Therefore, if used in practical calculations, PBP methods must be improved by the application of convergence-*accelerating* devices, of which more will be said later.

2.2.2 General remarks about linear-equation solvers

There are many highly impressive textbooks [6, 7] devoted to the available methods of solving linear algebraic equations. Their authors know vastly more about the subject than does the present one, whose experience nevertheless has highlighted factors that the textbooks fail to emphasize, as follows:

- The *merits of a solver* are to be measured primarily by the brevity of the *computer time* in which it needs to produce a set of x_i values that differ by less than a user-assigned tolerance from those that are ultimately found to satisfy all the equations exactly.
- A counterbalancing *demerit* may be (depending on the resources available) the magnitude of the *computer memory* that it requires.
- The *relative merits* of one solver to another depend enormously on the ratios of a_{ij} s to a_{ii} and to one another.
- They depend very greatly also on the distribution in space of the values of

$$x_{\text{Initial_guess}} - x_{\text{exact_solution}}$$

It would be unnecessary to make such statements were the literature not full of confident *unqualified* assertions regarding the superiority of one method to another. Nor had the author of one highly regarded 500-page textbook provided more than a mere five rather simple cases as tests for the comparison of the methods so learnedly described.

Moreover, the merits of methods are frequently assessed by reference to the magnitudes of the remaining *residuals*, that is, the magnitudes of e_I , defined by

$$e_I = a_{ii}x_i + \sum_j a_{ij}x_j - b_I$$

rather than in terms of the physically meaningful

$$x_{\text{computed}} - x_{\text{exact_solution}}.$$

It needs to be emphasized that residuals are imperfect measures of the quality of a solution. For example, a particular coefficient a_{ii} may be very large, as occurs when, so as to express one of the boundary conditions, one of the unknowns is being fixed by inclusion of a source term defined as

$$b_i = a_{ii}(x_{\text{fixed}} - x_{ii})$$

wherein x_{fixed} is the desired value. Then, even when x_{ii} differs from x_{fixed} by no more than round-off error, the product $a_{ii}(x_{\text{fixed}} - x_{ii})$ can appear as a residual of large size. It is the x_{ii} values that need to be considered, not residuals, and if the absolute value of $x_{ii} - x_{\text{fixed}}$ is less than the tolerance, that is, good enough.

It may be appropriate to voice some further observations concerning the linear equation solver literature at this point, namely, the following:

- It uses a known-only-to-devotees nomenclature, with no deference at all to the solver-*using* community.
- This nomenclature consists largely of surnames of authors: “Krylov subspace,” “Lanczos and Arnoldi iterations,” “Ritz approximation,” “Hessenberg form,” “Householder matrix,” etc. The “tridiagonal matrix algorithm” (see the succeeding text) is one of the few having memory-assisting significance.
- Although it is recognized that the equation sets frequently arise from the discretization of the differential equations of physics, the physical significances of their solutions are never disclosed.

2.2.3 The Thomas (or tridiagonal matrix) algorithm (i.e., TDMA)

Great importance attaches to the sets of equations that arise when the grid consists of a single chain of interlinked nodes, to which corresponds the reduced equation set:

$$a_i x_i + a_{I-1} x_{I-1} + a_{I+1} x_{I+1} = b_I$$

The reason is that there exists the well-known Thomas algorithm for solving the equations in question exactly *without iteration*. There is no need here to set out the details. It suffices to state that a finite number of operations, proportional to the number of unknowns, proceed from one end of the chain to the other and then back again. At the end of the sequence, all values of x_i are determined.

Of course, grids consisting of a single chain of nodes are rare; but the TDMA can be employed for two- and three-dimensional (3D) grids as well, albeit in an iterative manner. Consideration of how the TDMA then behaves will now be used to explain the influence of coefficient ratios on solver performance noted in [Section 2.2.2](#) in the foregoing. A 2D example suffices for which the typical equation can be written as

$$a_{I,j} x_{I,j} + a_{I-1,j} x_{I-1,j} + a_{I+1,j} x_{I+1,j} + a_{I-j-1} x_{I,j-1} + a_{I,j+1} x_{I,j+1} = b_{I,j}$$

wherein the subscripts containing i and j indicate node locations in the two coordinate directions.

It has been stated in the aforementioned that the PBP procedures treat the values on the right-hand side of their equations as temporarily known, which enables the left-hand side values to be updated. When the TDMA is applied to 2D problems, *one-half* of the right-hand side values are assumed to be known, that is, those in the second line of the equation; then, *all* the values in the first line can be determined.

Now, the importance of the coefficient ratios can be recognized; if the coefficients $a_{I,j-1}$ and $a_{I,j+1}$ are much smaller than the other a 's, the presumption that $x_{I-,j-1}$ and $x_{I,j+1}$ retained their previous iteration values is of no importance whatsoever. This could happen if the domain were very much larger in the j -direction than in the I -direction. The exact solution of the 2D problem would then be obtained without iteration.

What if the $a_{I,j-1}$ and $a_{I,j+1}$ are much *larger* than the other a 's? Then, the changes effected by the TDMA will be small, so that the process would have to be iterated many times to attain convergence. The use of an accelerating procedure would be very desirable.

2.2.4 Acceleration by overrelaxation

When the series of values of $x_{I,j}$, which are produced by a sequence of relaxations, is examined, it is usually found that the values are changing, iteration-by-iteration, in the right direction, but too slowly. It is tempting to “overrelax,” as it is often called, that is, to multiply the increments by some factor greater than unity. But how big should it be?

An obvious answer, which the present author happens *not* to have found in any textbook, is to compute the optimal factor by the following procedure:

- For the sets of $x_{I,j}$'s, both before and after relaxation, compute the residuals e_I .
- Apply increments of *twice the size* resulting from the relaxation and calculate the new residuals, that is, adopt tentatively an overrelaxation factor of 2.0.
- For each of the three sets of the residuals, compute the sums of their squares.
- Assume that the sums of the squares of the residuals vary in a quadratic manner with the relaxation factor (as they must). Hence, deduce what relaxation factor will produce the *minimum* sum.
- Adopt the new $x_{I,j}$'s that correspond to that factor and then make a new relaxation step.

This procedure always works, sometimes spectacularly; and it has been observed that it works better when the sums of the squares of e_I/a_{ii} are minimized rather than those of e_I itself. No claim is being made that it is better than others advocated in the rather large literature concerned with choosing optimal relaxation factors; but, about that literature, it should be remarked that no other front-runner has appeared.

The reason is that *mere* overrelaxation is not enough, for it applies somewhat better corrections at the locations to which less adequate corrections have *already* been applied but *only* to those locations. It takes too narrow a view of what needs to be done. This can be understood by consideration of Fig. 1.7, which illustrates what happens when the Jacobi PBP relaxation is employed.

The problem is that of one-dimensional (1D) heat conduction in a slab of uniform conductivity material, with its faces held at zero temperatures. The *initial guess* is represented by the two upper sloping lines; and the correct solution of the equations is the base of the triangle of which those lines are sides. It is easy to recognize that temperature corrections are needed everywhere; but a finite residual, that is, a heat imbalance, exists *only* at the location corresponding to the apex of the triangle; so, it is only there that the Jacobi relaxation makes any change.

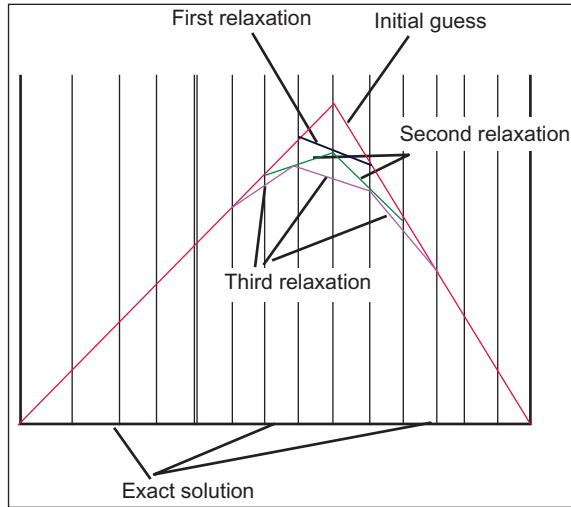


Figure 1.7 Graphic representation of a Jacobi solution process.

A Jacobi relaxation, expressed graphically, is a line drawn between nearby pairs of points across the spaces between them. Figure 1.7 shows the sets of lines for the first three relaxations. They have resulted, it might be said, in a “rounding” of the sharp-pointed initial triangle; but the third relaxation curve is still far from the final destination, namely, the zero temperature base.

Overrelaxation merely increases somewhat the cautious adjustments of Jacobi because of its self-imposed restriction of attention to points that currently report errors. What is needed is an acceleration procedure with a wider vision.

The same is true of much more sophisticated relaxation techniques such as Stone’s “strongly implicit procedure” [8]. Coupled with TDMA-based initial-guess improvers, such solver systems have for years provided satisfaction without any overrelaxation at all.

However, for whatever reasons, the attention of the linear equation solver specialist shifted long ago from overrelaxation toward acceleration methods of a different kind, now to be discussed.

2.2.5 Conjugate gradient solvers

In 1952, Hestenes and Stiefel [8] introduced the “conjugate gradient” method, which became for a time the leader of fashion. Its strategy was

1. to start with a guessed set of x_i values,
2. to calculate the associated residual e_I ,
3. to try another set of x_i 's and calculate *their* residuals,
4. to deduce from the two sets of $x_i \sim e_I$ pairs what would be a next try x_i that would probably reduce the sum of the squares of the residuals,
5. then to continue doing this until the sums became small enough.

The method (with various versions of step 5) appears to have had some success; but it was discovered, not surprisingly, that step 1 was the weak point. If one started a long way away from the final destination, the journey lasted appreciably longer.

2.2.6 Preconditioned conjugate gradient solvers

It was therefore decided by someone (who is unclear) (Question to readers #2: can anyone tell me, please?) to start by using a relaxation technique to improve the “initial guess.” No great attention was at first paid to which technique should be used; therefore, it was called, rather demeaningly, the *preconditioner*, as though it was something to be used at the start and then discarded.

But it was *not* in fact discarded; it was used again and again after each conjugate gradient “improvement”; and it was at last discovered that some preconditioners were much better than others. How much better, and in what circumstances, is hard to discover from the literature. Therefore, the present author, with Alexey Ginevsky of the Moscow Power Engineering Institute, is working to create a software package for studying the matter, as it might be said, experimentally.

Some preliminary results will now be shown. They relate to a 2D conduction problem in which temperatures at the boundaries of a square domain of uniform conductivity are held at temperature 0.0, while the initially guessed temperature at all other points is 1.0. The grid is a uniform $128 * 128$. The following images show temperature contours after each of 10 relaxer-plus-improver iterations, for six different solvers of conjugate gradient type (Fig. 1.8).

Clearly, there are very great differences in convergence behavior. The speed of convergence is successively greater for the first five solvers; but the sixth solver is probably not converging at all, because it is producing values of temperature that lie outside the range zero to one.

The names of the six solvers will not be disclosed here because the investigation, although still in its early stages, has already shown that the relative merits of the solvers are very dependent on the physical problem in question.

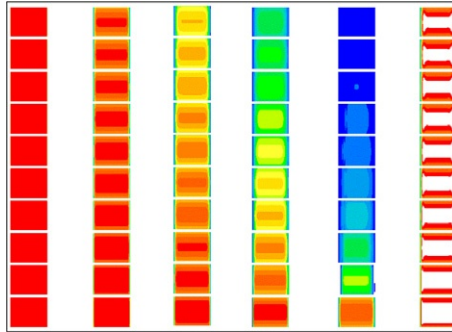


Figure 1.8 Temperature contours produced by six different solvers. First iteration at bottom, 10th at top. Colors mean: red $T=1$; blue $T=0$; white $T > 1$ or < 0 .

The purpose of presenting these preliminary results is simply to suggest that contributions to knowledge in this field can be made even by those who are not quite sure what a Krylov subspace actually is. If readers of this chapter wish to take part in the investigation, the software package (called Solvers Simulation Scenario) can be supplied to them.

2.3. Turbulence model trends

2.3.1 Origins

When the present author began his CFD career in the 1960s, the “turbulence model” concept perhaps did not exist, although examples did. Indeed, it may be that it was the publication of the book coauthored with Launder [9] that popularized it. For this reason, the author wishes to state that in his view, the pioneering publications were those of Boussinesq [10] in 1877, Prandtl [11] in 1925, Kolmogorov [12] in 1942, and Prandtl again [13] in 1945. All of these made their contributions before the advent of digital computers. After its advent, the first (and independent) pioneer was Harlow [14].

2.3.2 The effective-viscosity hypothesis

2.3.2.1 Early days

The contribution of Boussinesq was to *guess* that turbulent fluids were similar to laminar ones but possessed a much greater than laminar “effective” viscosity. It was a guess, not indeed very plausible to those who observed turbulent plumes of smoke in the environment; but it proved to be overwhelmingly seductive. If one could only find out what was the effective

viscosity at any location, the world of fluid dynamics would indeed be conquered!

Boussinesq's guess was a "try-on"; but it is now sufficiently venerable to be called a "hypothesis" and even a "model." The other just-mentioned pioneers all adopted it; indeed, it can be said that the purpose of their endeavors was to devise a means for predicting what value should be ascribed to the effective viscosity at any point within a turbulent flow.

2.3.2.2 The mixing length hypothesis

The laminar viscosity of a gas is known to be proportional to the mean free path of the molecules and to their average velocity; and it was by analogy with the mean free path that Prandtl [11] in 1925 introduced the concept of the "turbulent *mixing length*." He argued that momentum was transferred between adjoining layers of fluid, having different mainstream-direction velocities, by "parcels" of fluid that traveled a certain distance in a direction normal to that of the mainstream before mingling with and so transmitting momentum to the neighboring fluid.

Whatever the verbal argument employed, the result was the following formula for the effective (kinematic) viscosity:

$$v_{\text{eff}} = l_m^2 |du/dy| \quad (1.1)$$

where l_m is the mixing length and $|du/dy|$ is the absolute value of the local mainstream velocity gradient. This of course simply transfers the search for one unknown, v_{eff} , into the search for another, l_m , but Prandtl made two proposals with regard to the latter, namely, that

- close to a wall l_m was proportional to the *distance from* the wall, y , say, and
 - in limited extent turbulent flows remote from walls, such as jets, wakes, and plumes, l_m was proportional to the *distance across* the turbulent region.
- Values of the constants had to be deduced from experimental data, which was somewhat tiresome; but it could be tolerated if their variation from one situation to another proved not to be too great.

2.3.2.3 Two-equation turbulence models

In the early days of CFD (late 1960s), the mixing length hypothesis was gratefully seized upon, for example, by the many users of the GENMIX computer code [15]; and it proved to be nearly adequate for predicting the so-called "parabolic" flows within pipes and diffusers and in jets, wakes, and plumes. Even there, however, it was not entirely satisfactory, for example, the ratio of l_m to jet width proved to be 0.103 for plane jets and 0.075 for

axisymmetric ones. The search, therefore, began for some way in which the length scale or some other entity leading to v_{eff} , could be deduced.

The crucial advance appears to have been that of Kolmogorov [12], in 1942: he proposed that certain time-mean properties of turbulent flows could be deduced from the solution of *differential equations*. The dependent variables of these equations that he used were the

- kinetic energy of the fluctuating motion per unit mass, say k , and
- mass-average frequency of that motion, say f .

The terms in the equations were those to be found in all of conservation type, namely, time dependence, convection, diffusion, volumetric source, and volumetric sink.

Once k and f were known, Kolmogorov argued the effective viscosity could be deduced from

$$v_{\text{eff}} = Ck/f \quad (1.2)$$

where C would be a constant deducible from experimental data.

The work of Kolmogorov did not, in fact, become known to the scientific world until several years later, by which time a different two-equation model had become popular, namely, that of Harlow and Nakayama [14]. Its two dependent variables were the kinetic energy of the fluctuating motion, k , and the volumetric dissipation rate of that energy, ε ; and from these, the effective viscosity was to be deduced from

$$v_{\text{eff}} = Ck^{3/2}/\varepsilon \quad (1.3)$$

Both Kolmogorov's and Harlow's ideas were hopeful guesses, that is, "try-ons"; but it can be said that the latter's were rather more hopeful than the former's, because Kolmogorov proposed no positive source term for f , whereas Harlow proposed that the rate of generation of ε per unit volume and time should be proportional to k/ε times the corresponding rate of generation of k , that is, to the rate of energy generation by tangential and direct stresses.

The $k - \varepsilon$ hypothesis quickly and deservedly, because of its usefulness, acquired the more honorific appellation "model," to which indeed "classical" soon began to be added. Nevertheless, it is not disrespectful to raise an eyebrow concerning both Harlow's and Kolmogorov's choices of second dependent variable.

Their choice of turbulence energy k as a conserved property is understandable, for is not the first law of thermodynamics an energy conservation law? Indeed, Prandtl himself also proposed [13] a one differential equation

model in which the dependent variable was k . But conservation of f or ε ? Is it reasonable to suppose that two bodies of turbulent fluid, rapidly mixed together, will dissipate energy at the arithmetic mean of the two individual dissipation rates? Physics knows of no such law.

Interestingly, both Saffman [16] and the present author [17], independently of each other and of Harlow and Kolmogorov, proposed two-equation models with k as the dependent variable of the first equation; but as that of the second equation, they chose W , the sum of the squares of the *vorticity fluctuations*. That quantity, both authors believed, could reasonably be regarded as conserved: for vorticity *is* a conserved quantity.

Arguments were later advanced, and at the time thought persuasive, for preferring the Harlow–Nakayama choice. Years later, however, the same model was independently reinvented by Wilcox [18]; and it is now believed by some to be superior.

The history of turbulence modeling, viewed as a whole, can be seen as an equal-measure mixture of insight and accident. It is, therefore, interesting to speculate as to what might have transpired if Prandtl had happened to decide to make the mixing length l_m itself the dependent variable of his single differential equation. What other terms might he have had invented in order more or less to fit the known experimental data? A speculative answer is supplied in “Try-ons” in Section 4.1.

2.3.2.4 Wall functions

In the early days of CFD, computers had very limited memory; therefore, fine grids could not be afforded. Even for the small 2D parabolic problems dealt with at the start [19], it was recognized that calculating the effective viscosity appropriate to cells close to solid walls presented special problems. The topic appears as “wall-flux relationships” in the index of the foregoing reference. In the book on “elliptic flows” [20], which appeared 1 year later, the entry is “wall functions,” which is how it is usually referred to nowadays.

The wall functions used at that time were based upon experimental measurements rendered applicable to more general circumstances by expression in terms of dimensionless quantities. For the simplest possible circumstances, in which the relevant fluid properties (density and laminar viscosity) are constants, as is also the shear stress because of the absence of mass transfer and of pressure gradient, the effective viscosity in the near-wall layer can be expressed as

$$v_{\text{eff},n_w}/v_{\text{laminar}} = \gamma^+ / u^+ \quad (1.4)$$

where y^+ and u^+ are the dimensionless distance from the wall and along-wall velocity in the “law of the wall,” for which various empirically based expressions are available. The one that the present author particularly favors, because it covers the whole range in a single formula, [21] is

$$y^+ = u^+ + [e^{\kappa u^+} - 1 - \kappa u^+ - (\kappa u^+)^2/2 - (\kappa u^+)^3/6 - (\kappa u^+)^4/24]/E \quad (1.5)$$

where $\kappa = 0.417$ and $E = 0.86$.

Some empirically based formulas exist that express the influence of mass transfer through the boundary layer in reducing the effective viscosity, if the flow is *into* the fluid, and increasing it, if the flow is toward the wall, and also of the influences of pressure gradient and of roughness, but not when mass transfer and pressure gradient are *simultaneously* present. Practically nothing is known about the influences of nonunity viscosity and density.

Nearly half a century later, although the increase in computer power has been immense, wall functions are still in use. And the reason is still the same: even if computer power *does* suffice to allow use of arbitrarily fine grids close to walls, knowledge of the physics of low Reynolds number does not have the certainty or generality to make the expenditure worthwhile.

The point will not be expanded upon here; but it will be returned to later, first when “direct numerical simulation” is discussed and later in relation to “urban-terrain” simulation.

2.3.3 Reynolds stress models

Experience of using two-equation models was mixed. Engineers were pleased to have been supplied with computer programs that at least purported to handle turbulent flows at high Reynolds numbers. But the hopes of engineering scientists that a model would be found that fitted a wide range of phenomena, with very little ad hoc “tweaking” of constants, were disappointed. So the question arose: if two equations do not suffice, why not try using more?

Evidence had accumulated that one implication of the effective-viscosity hypothesis was not always correct: The shear stress and the velocity gradient did not always become zero at the same point; and why, anyway, should it be supposed that the effective viscosity, even if it did exist, would be direction-independent? These thoughts gave rise to the notion that the stresses themselves should be the dependent variables of differential equations; and this meant that, since the stress tensor has many components, *many equations* must be solved.

Here, it should be mentioned that the world of engineering science had changed immensely in respect to the number, and indeed nature, of the persons participating in it. Professors, students, theses, journals, and publications all proliferated, and so did the number and power of computers. Therefore, novelties in turbulence modeling, provided that they were not *too mind-testingly* novel, found many enthusiasts; and Reynolds stress models were prominent among them.

The present author has not studied the literature in detail; but to judge from the proceedings of the 2010 8th International Symposium on Engineering Turbulence Modeling and Measurement [22], it cannot be said that Reynolds stress models are as popular as they once were. Other “buzzwords” are at least as prominent in the titles and abstracts of the papers.

2.3.4 DNS

Among the said buzzwords is DNS, standing for direct numerical simulation, that is to say the solution of the unsteady *laminar* Navier–Stokes equations on a sufficiently fine grid and with sufficiently small time steps, for the details of turbulent-flow fluctuations to be accurately simulated. It is not a new line of study having been initiated in the 1970s (see Ref. [23] for a review of early work), and since computers have increased in power by many orders of magnitude since then, it is reasonable to expect that at least *some* useful results would have emerged.

What results could these be? Those referred to in Section 2.3.2.4 in the preceding text as being, regrettably, absent, namely, formulas for the effective viscosity of near-wall regions, as affected by pressure gradient, mass transfer, and nonuniform properties. It would not matter if these formulas were represented as provisional, because grid independence had not yet been demonstrated. At least the *trends* would be instructive. Yet, there is nothing so far as the present author can discover. One could suppose that the practitioners of DNS studies are not greatly interested in the production of results that others are waiting to use.

2.3.5 Large eddy simulation

Large eddy simulation (LES) is an even more prevalent buzzword than DNS. The underlying idea is that DNS requires finer grids and shorter time steps than even the largest of today's computers can accommodate. Very good! Let us use the finest grids and shortest time steps that we can afford; and for the finer-scale and more rapidly fluctuating phenomena, let us use conventional RANS (i.e., Reynolds-averaged Navier–Stokes, even the

now-by-some-despised $k-\epsilon$) modeling. Sometimes “hybrid” methods are employed, whereby the whole space is divided into regions, with RANS used in one and LES in another, the choice being made by the analyst so as to maximize the accuracy/effort ratio.

It is a rational strategy to embark upon, tentatively; and there have been many proofs that it enables realistic simulations to be made of flows, such as those behind a bluff body, which exhibit unsteady wake structures fluctuating periodically from side to side. The present author being an observer from a distance of this field of research makes only two remarks, namely, the following:

- It is evident from comprehensive publications such as Refs. [22, 24] that many variants of LES are being tried without the emergence of one that is widely acknowledged as superior to all.
- No attention appears to be being paid to the easy-to-activate ability of LES to produce the pdf (i.e., probability density function) information needed by heat transfer engineers for deducing volumetric averages of the nonlinear sources characterizing thermal radiation, for example, Ref. [24], admittedly confined to hydraulics applications, does not even include “pdf” in its index.

Thermal radiation is here mentioned because it is an example of a practically important physical process that, from the mathematical viewpoint, is *nonlinear*; for emission, it is proportional to the *fourth power* of the absolute temperature. This entails that a technique such as RANS, which can produce *only* time-averaged temperatures, cannot predict radiation well. LES, on the other hand, because it can compute for what proportion of time the temperature is by various amounts above and below the time-averaged temperature, can calculate the time average of the fourth power of the temperature. Reference [25] contains a full discussion of the possibility here alluded to. Its main message is that the *average* attributes of a population are rarely as interesting as the *departures from the mean*. It is only the strongest gusts of wind that fell the trees.

2.3.6 Population-based models

2.3.6.1 The main idea

That a turbulent fluid is to be regarded as a population is not a new idea. Prandtl, when introducing his mixing length hypothesis in 1925, clearly envisioned “parcels” of fluid having different velocities and directions of motion, which jostled with one another like members of an unruly crowd. The increasing prevalence of the notion in the nine succeeding decades can truly be recognized as constituting a “trend.”

Members of human populations can be distinguished by reference to many different attributes: Sex, religion, income, height, and corpulence may all serve; and they have differing importance according to whether one is seeking a wife, a basketball champion, or a sumo wrestler.

The same is true of turbulent fluids. Velocity is the attribute most pertinent to momentum transfer: temperature to thermal radiation, particle density to sifting processes, and chemical composition to combustion. Indeed, it is investigators of chemical reactions who have done most to foster the trend, as the following account will reveal. This account presents the highlights of a much longer review of the subject written in 2010 [26], together with those of some more recent material [27, 28].

Two important characteristics of populations, from the theoretical point of view, are *dimensionality* and *number* of members. If the only attended-to distinguishing feature of a group of men was their height, they would constitute a $1D$ population. If it were meaningful to pay attention also to their *weight*, their population would be classed as $2D$; and if the men were sorted additionally in respect to *age*, their dimensionality would be *three*. And so on without limit.

In this chapter, for the sake of concreteness, attention will be confined to $1D$ and $2D$ populations; and the fluid considered will be a turbulent mixture of gaseous fuel, air, and their products of combustion. As to the number of members, it will be found that valuable information can sometimes be provided by considering populations with as few as *two* members. However, the richness of information increases, as a rule, with the number of members considered, just as is true of the fineness with which the dimensions of the distance and time are discretized in conventional CFD.

2.3.6.2 Graphic representations

Population distributions can be conveniently displayed graphically, whereby it is to be noted that they have their idiosyncrasies. Thus, the single vertical line in Fig. 1.9 represents, by the horizontal position of the single red line of unity height, the local and instantaneous temperature of a single-member population of fluid, that is, of a fluid such as is envisaged by conventional turbulence models.

Figure 1.10, by contrast, represents what might be the same turbulent fluid by means of six lines at arbitrarily selected temperatures, the vertical lengths of which represent proportions of time within which each the fluid is supposed to possess the temperature corresponding to the horizontal position of the line. It is somewhat similar to a pdf, which is a histogram, with

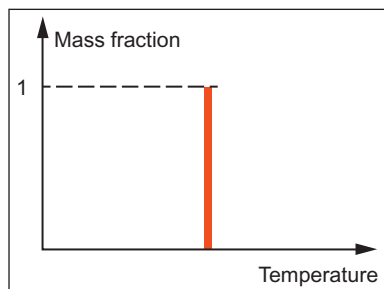


Figure 1.9 One-member.

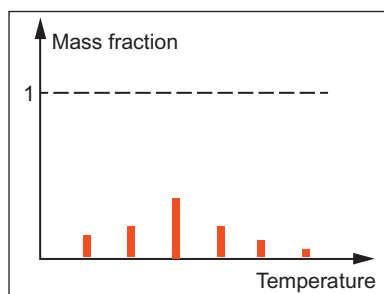


Figure 1.10 Six-member.

contiguous vertical strips rather than vertical lines; it differs in that temperature is being thought of as “quantized,” in the sense that fluid with between-the-lines temperature is imagined never to exist at all.

Figure 1.10 relates to a $1D$ population, for temperature is all that distinguishes one member from another. The strict $2D$ counterpart would be a plane, having temperature, say, as its abscissa and fuel concentration, say, as it ordinates. Then, the quantized temperature–concentration pairs would appear as dots scattered regularly or irregularly over its surface; and the mass fractions of mixture material associated with each state, corresponding to the lengths of the vertical lines in the $1D$ diagrams, would have to be represented by the diameters of the dots.

Because of the eyesight strain that such a practice would impose, it is not used. Instead, easier-to-draw-and-read *contour* diagrams will be used, in which practice tends to blur the distinction between population distributions and pdfs that had just been made. However, it is only to the persons writing the corresponding computer programs that the distinction is

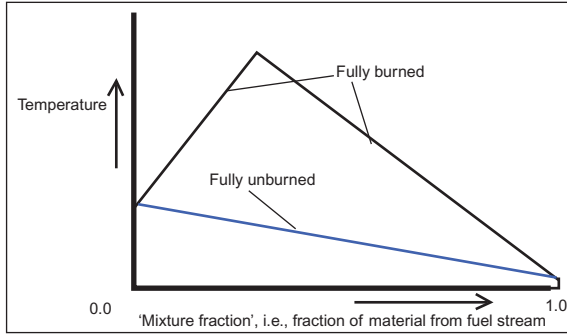


Figure 1.11 Extremes of temperature.

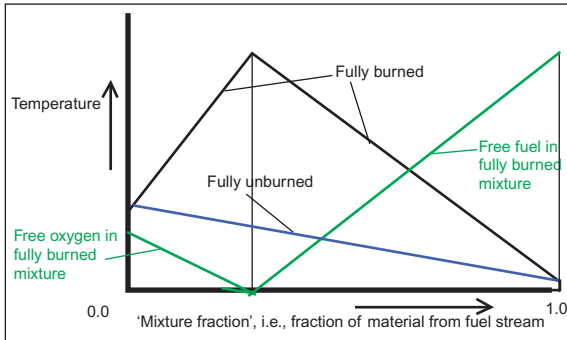


Figure 1.12 Extremes of concentration.

important; so it will not be referred to again here. Before the 2D representation is introduced, however, two other diagrams are worth inspecting.

Figure 1.11 shows how the *temperature* of a fuel–air mixture varies with the fuel proportion, when the fuel is (upper, two lines) fully *burned* and (lower, one line) fully *unburned*. The *adiabatic temperature rise* is the vertical distance *between* the upper and lower lines.

Figure 1.12 shows the *free-fuel* and *free-oxygen* values for the fully burned condition. The mixture fraction at which both oxygen and fuel are zero is called “*stoichiometric*.”

2.3.6.3 The “TriMix” diagram, a “map” of fuel–air–combustion product states

The “TriMix” diagram, now to be described, is a way of mapping the states that lie *between* the fully burned and fully unburned extremes. Its *vertical*

dimension is the *adiabatic* temperature rise resulting from complete combustion of the fuel (to CO_2 and H_2O), hence, the “Tri” in its name. Its *horizontal dimension* is the mass fraction of fuel-derived material or, *in atomic terms*, $(1.0 - \text{atomic_nitrogen_fraction}/0.768)$. Points lying outside the triangle correspond to *nonphysical* negative concentrations. They can, therefore, be ignored. The TriMix diagram made its first published appearance in Ref. [27] (Fig. 1.13).

The TriMix diagram will be used as a means of describing the states of turbulent gas mixtures. But, first, its ability to display simple balance-based properties of state will be illustrated by way of five contour diagrams in Fig. 1.14. Any other properties, such as density and viscosity, can also be computed and displayed as well as, if chemical kineticists are to be believed, the rates of chemical reaction.

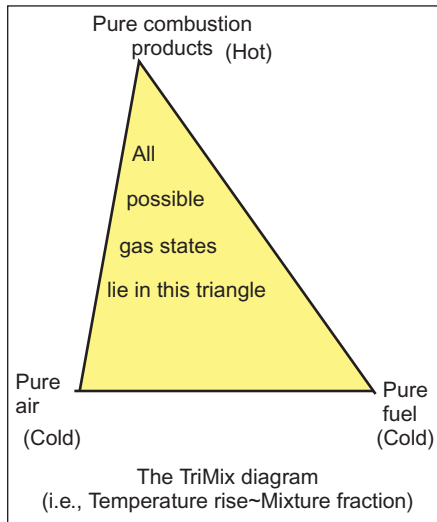


Figure 1.13 The TriMix map.

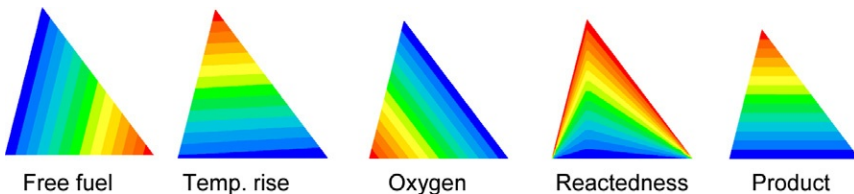


Figure 1.14 Contours displaying gas states on TriMix.

There are *three kinds* of reaction to be considered, of which the *rate contours* are shown (red is high rate; blue is low rate) (Fig. 1.15).

Of these reactions, the first is usually desired, being the main producer of energy, whereas the other two are usually undesired, for they produce air pollutants. The designer of a combustor therefore would like to know *where* on the TriMix diagram his hottest gases lie. Preferably, it should be in the stoichiometric-mixture -ratio region; for oxides of nitrogen are generated if the mixture ratio is too lean there and smoke is generated if it is too rich. It should be understood that so far, no particular flame has been considered but knowledge has been assembled about the attributes of *all possible members* of the gases-in-flame population.

2.3.6.4 The combustor-simulation problem

Figure 1.16 shows a TriMix diagram that *could* in principle represent a particular flame or rather a particular location within it, for its contours are those of *the proportions of time* in which the gas at that location is in each of the possible *states represented on the state map*. If he possessed such a diagram for a sufficient number of locations within his combustor, the combustor designer

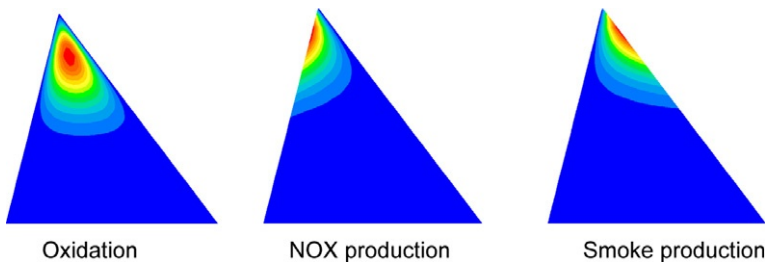


Figure 1.15 Rate contours.

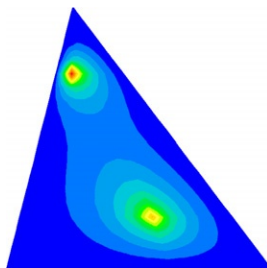


Figure 1.16 2D population distribution.

would be able to deduce *total* rates of the three reactions. To provide him with such knowledge is the task of the CFD specialist, who will, of course, need a populational model of turbulence for the purpose.

2.3.6.5 When the turbulent fluctuations are ignored

Very few indeed are the CFD specialists who even know of the existence of such models, let alone use them. It is common still to ignore the fluctuations of concentration entirely, thus in effect presuming that the state of the mixture at a particular location in the combustor is represented by a single point on the TriMix map, as shown in Fig. 1.17.

Two finite-volume equations have to be solved so as to determine the position of the point on the map: one for *mixture fraction* and one for *unburned fuel fraction*. It is better than nothing; but it is not very good. A one-member population is no population at all.

2.3.6.6 EBU: the first two-member population model

The first-ever turbulent-combustion model that took meaningful account of fluctuations appears to have been the so-called eddy break-up" (EBU) model of 1971 [29]. This postulated a population of *two members*, both having the same *fuel ratio*, with *one fully burned* and the other *fully unburned*. The two members were supposed to collide, at rates fixed by hydrodynamic turbulence, forming intermediate-temperature and intermediate-composition material that quickly became fully burned. This model provided a (negative) source term in the finite-volume equation for the unburned fuel fraction, often expressed as

$$\text{source} = -\text{constant} * \text{density} * r * (1 - r) * \varepsilon / k \quad (1.6)$$

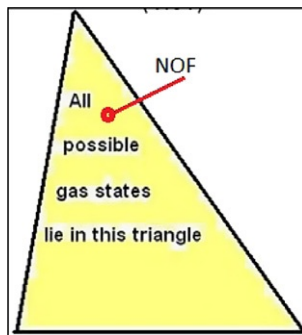


Figure 1.17 The no-fluctuations presumption.

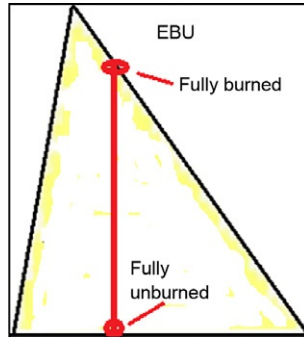


Figure 1.18 EBU on the TriMix map.

where r is the local reactedness of the mixture, so that r : $(1 - r)$ is the ratio of burned to unburned material, and ε and k are from the $k - \varepsilon$ model of hydrodynamic turbulence (Fig. 1.18).

The EBU was successful in explaining some puzzling experimental data regarding the almost-constant angle of turbulent premixed flames in the wake of bluff bodies in plane-walled ducts; and the link that it made between the combustion rate and the hydrodynamics of the flow has found its way into almost every subsequent model of turbulent combustion.

2.3.6.7 A two-member model with Navier–Stokes equations for each member

In the 1970s, problems connected with the steam generators of pressurized-water-cooled nuclear reactors stimulated the development of methods of numerical simulation of two-phase flows. This involved the formulation and solution of two sets of interlinked Navier–Stokes equations, one for each phase. Such an algorithm was IPSA (Inter-Phase-Slip Algorithm) [30].

Although conceived with intermingling steam and water in mind, the algorithm could just as easily be applied to the hotter and colder gases that were envisaged in the EBU concept and without its overrestrictive assumption that they must be fully burned or fully unburned. Such a study is reported in Ref. [31], which describes how a shock wave passes along a horizontal pipe containing a combustible gas that is burning slowly.

The wave accelerates the hot-gas fragments more than the cold ones, causing relative motion. The relative motion causes increased entrainment and mixing, which increases the burning rate. This increases the strength of the pressure wave. The result is that the deflagration turns into a detonation (Fig. 1.19).

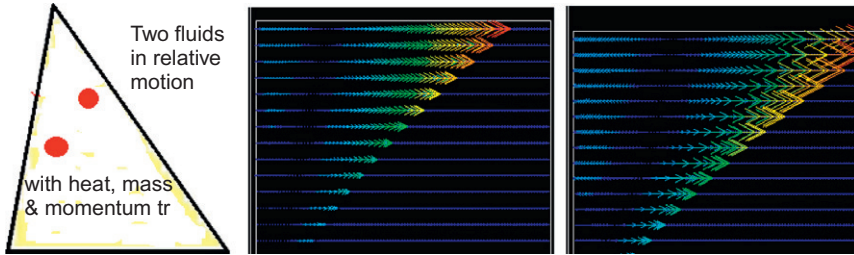


Figure 1.19 Instantaneous TriMix state and successive velocity vectors of colder and hotter members of the two-member population (time increases with vertical position).

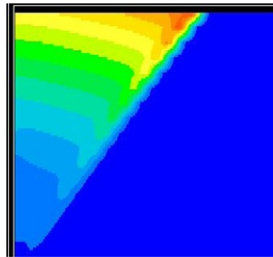


Figure 1.20 Pressure contours, distance horizontal, and time vertical.

Figure 1.20 shows the corresponding contours of pressure, which is shared by both gases.

These calculations were performed in 1983; but, for accidental historical reasons, little attention was paid to further development of the model at that time. Now that the ability to predict two-phase flow with interphase slip is more widely spread, it is hoped this chapter may awaken wider interest.

2.3.6.8 A four-member population model

The puzzling facts about turbulent premixed flames in plane-walled ducts, alluded to earlier-mentioned, were

- increasing flow velocity increases flame speed so the flame angle remains constant and
- sufficient increase of velocity *extinguishes* the flame.

EBU, that is, a *two*-fluid model, explained the first, but not the second. The solution [32] (24 years later!) was this: refine the (populational) grid. In other words, use a *four*-fluid model (Fig. 1.21).

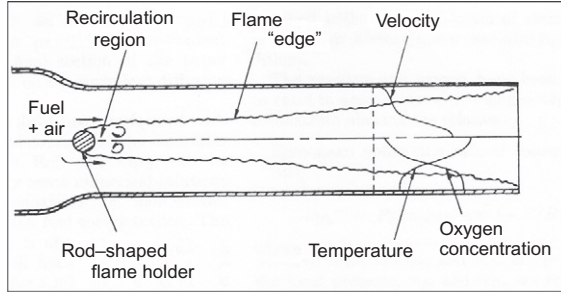


Figure 1.21 The Scurlock [33] experiment that prompted the invention of EBU.

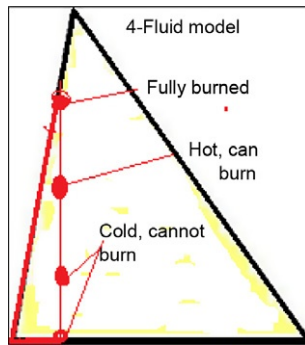


Figure 1.22 TriMix representation of the four-fluid model.

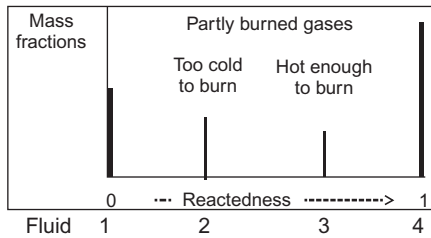


Figure 1.23 Mass fractions of the four population members.

The presence of the *hot, can burn* fluid (see Fig.1.22) allows space for chemical-kinetic limitations to enter. So extinction can be predicted (in principle). The EBU postulate was that fully burned and fully unburned gas fragments collided, at concentration-proportional rates, and the mixture combusted instantly; but with four fluids, there are more pairings possible and, therefore, more varied behavior (Fig. 1.23).

The physical presumptions are that

- fluids 1 and 4 collide at a hydrodynamically controlled rate, like Prandtl's "parcels," producing fluids 2 and 3;
- fluids 1 and 3 also collide to produce fluid 2;
- fluids 2 and 4 collide to produce fluid 3.

This fluid, being hot enough to burn, diminishes in mass fraction at a chemical-kinetically controlled rate, which is why that of fluid 4, the product of combustion, correspondingly increases.

Of course, a four-member population is "too coarse a grid" to permit accuracy, for reaction rates vary with temperature (i.e., reactedness) in a highly nonlinear manner, such as that of Fig. 1.24, wherein the fall to zero at high temperature results from the complete consumption of the reactants.

For such a curve, probably as many as twenty fluids would be needed, if their reactedness intervals were uniform, to achieve acceptable numerical accuracy. But why *not* have 20? Or more?

2.3.6.9 The multimember population

Long though it had taken to move from two to four fluids, the advance to multimember populations proceeded swiftly, both 1D and 2D populations being investigated. Reference [26] provides access to many of the early results, of which only the following set of four will be shown here. In order to point out that *how many* members are needed can be determined by trial-and-error. "Grid-refinement" studies are as practicable (and necessary) for populational grids as they are for spatial or temporal ones.

The same is true of discretized populations. *Grid-refinement* studies, as shown in Fig. 1.25, must be made for a 2D population at one particular geometric location in a flame with reactedness as the vertical dimension and mixture fraction as the horizontal one (TriMix not having been invented at the time).

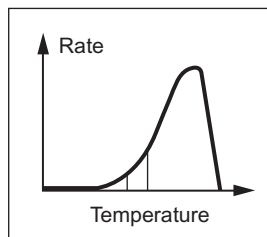


Figure 1.24 Typical variation of reaction rate with temperature.

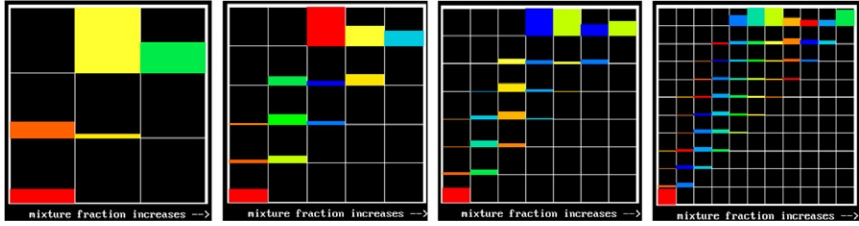


Figure 1.25 Predicted population distributions for 3^*3 , 5^*5 , 7^*7 , and 11^*11 .

At this point, it is appropriate to disclose that there does exist another approach to modeling turbulent combustion that can also be properly called “populational”: it is that which is usually referred to as “pdf transport.” The concept was first put forward in 1974 by Dopazo and O’Brien [34] in analytical form; then, in 1982, Pope [35] expressed it numerically. However, the chosen numerical method was a version of the Monte Carlo method, the unfamiliarity of which to most CFD specialists has perhaps hindered its acceptance and further development.

Because its associated computer times are rather long, it is unfortunate that the Monte Carlo lacks the time-saving grid-refinement (and grid-coarsening) capability of the discretized-population approach, which is advocated here. The latter provides non-absurd results even with a nine-cell grid, as has just been seen; but the corresponding “nine-particle-group” version of the Monte Carlo method would give no information that could be relied upon at all.

2.3.6.10 Populational and conventional CFD compared

It is now necessary to explain in more detail how such population-distribution diagrams are constructed. Let the colored-area proportion of each box, representing the mass fraction of the population that possesses the corresponding pair of attributes, be represented by the symbol $m_{i,j}$. Then, $m_{i,j}$ obeys a differential equation of the familiar “conservation” form:

$$\partial(\rho m_{i,j})/\partial t + \text{div}(\rho_1 \mathbf{v}_{i,j} m_{i,j}) = \text{div}(\Gamma_{i,j} \text{grad} m_{i,j}) + S_{i,j} \quad (1.7)$$

in which the four terms represent time dependence, convection, (turbulent) diffusion, and sources in the usual way.

Although the *form* of the equation is familiar, there are several unusual features to be remarked upon:

- The subscripts i, j , which attach to the velocity vector \mathbf{v} , are a reminder that different population members may possess different velocity components, as was seen in Fig. 1.18 where the same pressure gradient had very different effects on the hotter and colder gases.
- The source term has to express mathematically two quite distinct processes, only one of which, namely, chemical reaction, is recognized by conventional CFD.
- Even this has to be differently expressed, namely, as a *diminution* in the mass fraction of lower-reactedness members of the population and an *increase* in mass fraction of higher-reactedness members.
- The process for which conventional CFD has no counterpart is that expressed earlier as “collision” between more remote members of the population and consequent “production” of material of intermediate attributes. Moreover, a new hypothesis has to be invoked in order that sources and sinks can be evaluated, for example, as a generalization of Eq. (1.6), in which the $r(1-r)$ term can be recognized as the product of the mass fractions of the two members of the population.
- Figure 1.26, extracted from Ref. [36], will enable the reader to envision the possibilities.

These differences from conventional CFD are not such as to present any computer-coding difficulty. *Any* commercial CFD code, therefore, provided that it allows its users to add source terms and make minor modification to built-in diffusion and convection formulations, could be employed for solving the populational turbulence model equations. Why, therefore, is this seldom, if ever, done? The present author has no satisfactory answer to that question.

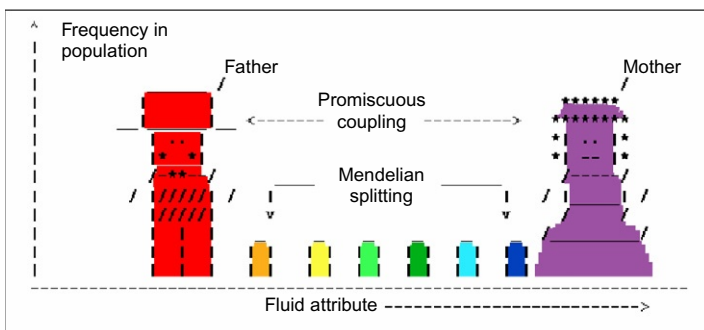
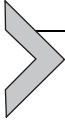


Figure 1.26 Illustration of the “promiscuous-Mendelian” hypothesis.



3. TRICKS

3.1. The IMMERSOL radiation model

3.1.1 *The magnitude of the radiative problem*

Turbulence, chemical reaction, multiphase flow, and radiation are the four main phenomena for which CFD practitioners make use of “*models*,” that is, of mathematical idealizations that, although known to fall far short of complete representations, may still, in favorable circumstances, permit useful predictions to be made. Of these,

- the first receives great attention from CFD specialists and enjoys high respect as an engineering science challenge;
- the second is the active concern of, perhaps, an even greater number; and
- the third, though presenting fewer downright mysteries, is the subject of continued and large-scale research.

Radiation, however, although presenting comparable difficulties, has been a less popular subject for research. As a consequence, inability to model radiation realistically is often the *main cause of inaccuracy* in CFD predictions.

This is understandably true of high-temperature processes, such as those in the combustion chambers of engines and furnaces; but it is no less true of lower-temperature ones. Situations in which convective, conductive, and radiative modes of heat transfer may all have similar orders of magnitude include electronic equipment and the living accommodation of human beings.

Radiative heat transfer can be described mathematically with exactness. Perhaps for this reason, it is commonly supposed that enabling a CFD code to add radiation to its predictive capabilities is simply a matter of selecting and attaching to it one or other of the available equation-solving methods. These go under the names of Monte Carlo, discrete transfer, discrete ordinate, zone, etc.

Unfortunately, consideration of how these methods actually perform, when applied to problems of more than modest size, makes plain that they must *all* require very much more computer and elapsed time than anyone can afford. This is so even with neglect of the influences of

- wavelength on absorption and emission,
- impingement angle on the reflectivity of surfaces,
- temperature on the radiative properties of materials,
- chemical composition and “surface finish” of those materials, and
- the complicating presence of turbulent fluctuations of temperature and of multiphase flow.

3.1.2 *The action-at-a-distance difficulty*

Radiative heat transfer differs in character from conductive and convective heat transfer in that it involves “action at a distance.”

Heat *conduction* to a point is influenced by the temperatures of the materials at the immediately *surrounding* locations. Heat *convection* to a point is influenced by the temperature on the immediately *upstream* side. Heat radiation, by contrast, can depend on the temperatures *at all surrounding points*, no matter how far away they are. Admittedly, the more remote points usually have less influence than the nearer ones; but the temperature of the sun affects the heat flux to Earth, that is, remote enough by human standards.

One way of expressing the difference between various modes of heat transfer is to state that the “mean free path of radiation” is often much larger than the dimensions of the domain of study. The “mean free paths of conduction and convection,” on the other hand, are usually much smaller, being of the order of the distance between molecules or (in turbulent flow) of the size of the smallest eddies. That of radiation varies inversely with the amount of radiation-absorbing material per unit path length, which is why it is so large in “outer space,” where there is no such material.

Where, however, *much* radiation-absorbing material is present, for example, within a furnace, where pulverized-coal particles and finely divided soot absorb scatter and reemit radiation, the mean free path of radiation *can* be much smaller than the apparatus dimensions. Then, radiative transfer can be regarded as similar to heat conduction, but with an increased thermal conductivity.

The “trick,” which will now be described, is to treat radiation through *empty* space as though it there too behaved in a conduction-like manner. It is embodied in the so-called [54] IMMERSOL (i.e., immersed solid) model of radiation. Since this, although much used by the present author and his colleagues for many years, has never been adequately described in print, the omission will now be rectified.

3.1.3 *IMMERSOL: the main features*

3.1.3.1 The dependent variables

IMMERSOL distinguishes three temperatures for a control volume in a medium, which is transparent to radiation, namely,

- T_1 , the temperature of the first phase, for example, air;
- T_2 , the temperature of the second phase, if present, for example, a cloud of solid particles suspended within the air; and
- T_3 , the “radiosity temperature” defined in the succeeding text.

If R stands for the *radiosity*, that is, the sum of all radiation fluxes traversing the control volume, regardless of direction and wavelength, then T_3 is related to it by the equation

$$R = \sigma T_3^4$$

where σ is the Stefan–Boltzmann constant ($5.670373 \times 10^{-8} \text{ W m}^{-2} \text{ K}^{-4}$) and T_3 is measured in degrees Kelvin, as are the other temperatures. Therefore,

$$T_3 = \sigma^{-1} R^{1/4} \quad (1.8)$$

3.1.3.2 The differential equations

The variables T_1 and T_2 obey differential equations of the familiar conservation kind, distinguished by special source terms, thus,

$$\partial(c_1 \rho_1 T_1) / \partial t + \text{div}(c_1 \rho_1 \mathbf{v}_1 T_1) = \text{div}(\lambda_1 \text{grad} T_1) + S_{1,2} + S_{1,3} \quad (1.9)$$

and

$$\partial(c_2 \rho_2 T_2) / \partial t + \text{div}(c_2 \rho_2 \mathbf{v}_2 T_2) = \text{div}(\lambda_2 \text{grad} T_2) + S_{2,1} + S_{2,3} \quad (1.10)$$

wherein

- $S_{1,2}$ and $S_{2,1}$ represent energy transfers per unit volume between phases one and two;
- \mathbf{v} represents the velocity vector;
- $S_{1,3}$ and $S_{2,3}$ represent volumetric rates of radiative heat absorption and emission;
- λ_1 and λ_2 represent the sums of the thermal conductivities, laminar plus turbulent, of the respective phases;
- c represents specific heat;
- ρ represents density; and
- t represents time.

T_3 obeys a similar equation but with fewer terms. Specifically, it has a zero on the left-hand side because radiation is not convected in either time or space. Its equation is

$$0 = \text{div}(\lambda_3 \text{grad} T_3) + S_{3,1} + S_{3,2} \quad (1.11)$$

3.1.3.3 The source terms

About $S_{1,2}$ and $S_{2,1}$, nothing needs to be said here except that they represent the interphase transfer processes in the usual way. It is the $S_{1,3}$, $S_{2,3}$, $S_{3,1}$, and

$S_{3,2}$ terms that require discussion. The IMMERSOL presumption is that they are related to the three temperatures via the following equations:

$$S_{1,3} = -S_{3,1} = \varepsilon'_1 \sigma (T_3^4 - T_1^4) \quad (1.12)$$

and

$$S_{2,3} = -S_{3,2} = \varepsilon'_2 \sigma (T_3^4 - T_2^4) \quad (1.13)$$

wherein ε'_1 and ε'_2 are the emissivities of their respective phases per unit length. These quantities are supposedly numerically equal to the absorptivities, which measure the proportion of the radiation flux that is absorbed per meter of its passage through the medium in question.

3.1.3.4 The value ascribed to λ_3

IMMERSOL expresses the thermal conductivity pertaining to the radiosity temperature T_3 in terms of the emissivities per unit length ε' and the scattering coefficients per unit length s' of the two phases in the transparent-to-radiation space and the gap between nearby solid walls W_{gap} as

$$\lambda_3 = 4\sigma T_3^3 / \{0.75(\varepsilon'_1 + s'_1 + \varepsilon'_2 + s'_2) + 1/W_{\text{gap}}\} \quad (1.14)$$

The origin of this equation, and the meaning of W_{gap} , will be explained in the succeeding text.

3.1.3.5 The boundary conditions

At the walls of, and everywhere within, solid bodies surrounding or immersed in the transparent medium, T_3 is taken as being equal to the temperature T_1 or T_2 , according to the phase in question. However, the radiant flux at such walls depends not only on the T_3 gradient in the medium close to the wall but also on the surface emissivity of the wall itself, in a manner that will be discussed in [Section 3.1.4.4](#). At open boundaries of the domain, net radiation fluxes are ordinarily prescribed.

3.1.4 IMMERSOL: the rationale

3.1.4.1 Starting points

In its neglect of wavelength dependency, the IMMERSOL model departs radically from reality; but it does so in a manner that is commonly regarded as acceptable: it employs the widely used “gray-medium” approximation described in many textbooks, for example, in Sparrow and Cess [38].

In that book, and elsewhere, two other accepted concepts are described that IMMERSOL has adopted, namely, those of the *optically thick* and *optically thin* limits. Here, “thick” and “thin” compare the size of the gap between the solid walls enclosing the transparent medium with what can be called the “mean free path” of radiation in that medium, that is, the reciprocal of $(\epsilon' + s')$. What is distinctive about IMMERSOL is that it is valid both *at* and *between* those limits.

Both extremes arise in practice. Within a large coal-fired furnace, the cloud of burning particles and gaseous combustion products can be regarded as optically thick, for so much solid surface is present per unit volume that rays emanating from the middle of the furnace must be multiply reflected before they escape to the water-cooled walls. The air within the rooms and corridors of inhabited buildings, by contrast, constitutes an optically thin medium; wall-to-wall radiation suffers no impediment.

For optically thick media, there exists a formula that connects the radiative heat-flux vector \mathbf{q} , in W m^{-2} , with the gradient of the radiosity. It is usually associated with the name of Rosseland [39], and it is

$$\mathbf{q} = -(4/3)(\epsilon' + s')^{-1} \sigma \text{grad}(T^4) \quad (1.15)$$

Here, T is the local temperature of the transparent medium.

If the equation is expressed in terms of an effective thermal conductivity λ_{eff} , involving $\text{grad}T_3$ rather than $\text{grad}(T_3^4)$, the expression for λ_{ref} becomes

$$\lambda_{\text{eff}} = (16/3)(\epsilon' + s')^{-1} \sigma T_3^3 \quad (1.16)$$

At the other extreme, when the medium is so thin as not to participate at all in the radiative heat transfer between two solid surfaces, at temperatures $T_{3\text{hot}}$ and $T_{3\text{cold}}$, say, the heat flux \mathbf{q} is well known to obey the formula

$$\mathbf{q} = \{1 + (1 - \epsilon_{\text{hot}})/\epsilon_{\text{hot}} + (1 - \epsilon_{\text{cold}})/\epsilon_{\text{cold}}\}^{-1} \sigma (T_{3\text{hot}}^4 - T_{3\text{cold}}^4) \quad (1.17)$$

Equation (1.15) is of the flux-proportional-to-gradient kind that CFD codes are well equipped to solve. Equation (1.17) is of the less amenable action-at-a distance kind. The question arises: how can the latter be made more like the former?

3.1.4.2 First steps

Rewriting Eq. (1.17) for the case in which $(T_{\text{hot}} - T_{\text{cold}})$ is small and *in which the wall emissivities are unity* yields

$$q = 4\sigma T^3(T_{\text{hot}} - T_{\text{cold}}) \tag{1.18}$$

where T stands for either temperature because they are nearly equal.

Since the temperature gradient equals $(T_{\text{hot}} - T_{\text{cold}})/W_{\text{gap}}$, the effective conductivity that corresponds to Eq. (1.18) is simply

$$\lambda_{\text{eff}} = 4W_{\text{gap}}\sigma T^3 \tag{1.19}$$

where W_{gap} stands for the distance between the solid surfaces. So, the conductivity increases with interwall distance, as it must do if the heat flux is to be independent of that distance.

It is interesting to compare the value of this conductivity with the thermal conductivities of common materials as seen here:

Atmospheric air	Water at 0 °C	Steel
0.0258	0.569	43.0

wherein the units are $\text{W m}^{-1} \text{ }^\circ\text{C}^{-1}$.

In the same units, and with a wall gap equal to 1 m, the values of λ_{eff} at various temperatures in degrees Celsius are

T_3	20	100	500	1000	1500	2000
λ_{eff}	5.706	11.77	104.8	467.9	1264.1	2663.6

Even taking into account that turbulence may increase the effective conductivity of a fluid by two or three orders of magnitude, it can be concluded from these tables that radiative heat transfer can be significant at room temperature and that at high temperatures, it becomes dominant.

3.1.4.3 Between the “thick” and “thin” extremes

Let now the *reciprocal* of conductivity be considered, that is, the resistivity, $\lambda_{\text{eff}}^{-1}$, measured in $^\circ\text{C m W}^{-1}$. For the thick medium, Eq. (1.16) yields

$$\lambda_{\text{eff}}^{-1} = (3/16)(\varepsilon' + s')(\sigma T^3) \tag{1.20}$$

and, for the thinnest-possible totally empty medium, Eq. (1.19) yields

$$\lambda_{\text{eff}}^{-1} = 1/(4W_{\text{gap}}\sigma T^3) \tag{1.21}$$

It is, therefore, not unreasonable to suppose that, for intermediate conditions, the two multipliers of σT^3 should be *added* so as to create a more generally valid single resistivity formula, thus

$$\lambda_{\text{eff}}^{-1} = \left\{ (3/4)(e' + s') + 1/W_{\text{gap}} \right\} / (4\sigma T^3) \quad (1.22)$$

This is the source of Eq. (1.14), introduced in Section 3.1.4, and it can be described as the first part of the “IMMERSOL trick.” But there is more to come.

3.1.4.4 Wall emissivity as an extra resistance

Equation (1.14) is used in IMMERSOL to calculate the T_3 diffusion fluxes of the finite-volume equations, which CFD codes easily solve. However, something special has to be done for coefficients when one node lies in the transparent medium and the other within a solid, as exemplified by nodes B and A in the Fig. 1.27, in which, for simplicity, the transparent medium consists of a single phase.

As is usual in CFD codes, the conductivities pertaining to the cell are stored at each grid node. Therefore, the radiative heat flux crossing the boundary between cells B and C will be deduced from the formula:

$$\text{flux}_{B \text{ to } C} = (T_{3,B} - T_{3,C}) / \left\{ (x_I - x_B) / \lambda_{3,B} + (x_C - x_I) / \lambda_{3,C} \right\}$$

where x is the horizontal coordinate.

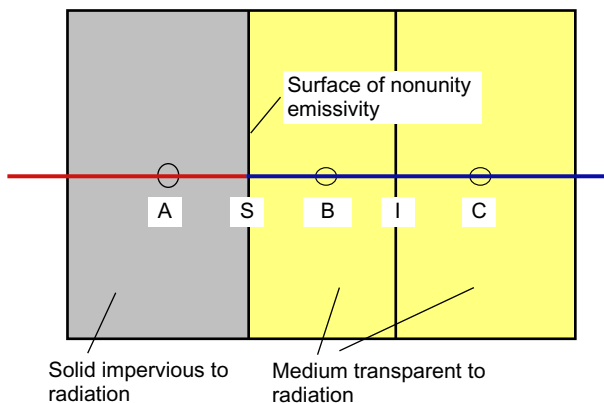


Figure 1.27 Computational cells near-solid surface.

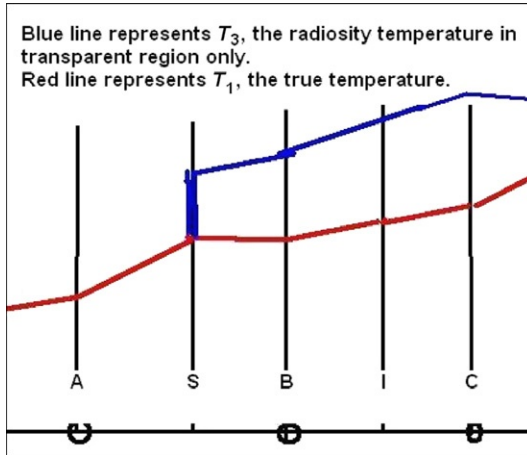


Figure 1.28 T_1 and T_3 profiles near a solid surface.

The calculation of the radiant flux at the S interface, however, requires more careful study because the surface emissivity can cause a discontinuity of T_3 gradient there, as is illustrated in Fig. 1.28, which shows the postulated profiles of *both* T_3 and T_1 because of their inescapable interaction.

Here, it is postulated that T_3 and T_1 are equal to each other within the solid; but, whereas the latter has a finite gradient everywhere, the former may have an infinite one at the interface between the phases. The fluxes of energy in question are as follows:

- Conduction from A to S , namely, $(T_{1,A} - T_{1,S})\lambda_{1,A}/(x_S - x_A)$
- Conduction and convection from S to B , namely, $(T_{1,S} - T_{1,B})\lambda_{1,B}/(x_C - x_S)$
- Radiation from S to B , namely, $(T_{3,S} - T_{3,B})/\{(x_C - x_S)/\lambda_{3,B} + (1 - \varepsilon_S)/\varepsilon_S\}$ wherein the term involving ε_S is inserted so as to conform with Eq. (1.17) in the preceding text. This is the second part of the “IMMERSOL trick.”

Requiring the fluxes to be in balance at the surface S enables the equal-by-definition values of T_3 and T_1 there to be evaluated. The necessary formula is as follows:

$$\begin{aligned}
 T_{1,S} &= T_{3,S} \\
 &= \left\{ T_{1,A}\lambda_{1,A}/(x_S - x_A) + T_{1,B}\lambda_{1,B}/(x_B - x_S) \right. \\
 &\quad \left. + T_{3,B}/\{(x_B - x_S)/\lambda_{3,B} + (1 - \varepsilon_S)/\varepsilon_S\} / [\lambda_{1,A}/(x_S - x_A) \right. \\
 &\quad \left. + \lambda_{1,B}/(x_B - x_S) + 1/\{(x_B - x_S)/\lambda_{3,B} + (1 - \varepsilon_S)/\varepsilon_S\}] \right\} \quad (1.23)
 \end{aligned}$$

3.1.5 IMMERSOL: conclusions

The equations now assembled have transformed the problem of numerically simulating radiative heat transfer into one that can be solved by any computer code capable of handling conductive and convective heat transfer. The fields of T_3 can now be computed, and the radiant heat flux vector \mathbf{q} at any point can be deduced from its gradient via

$$\mathbf{q} = -\lambda_3 \text{grad} T_3, \quad (1.24)$$

with λ_3 calculated from Eq. (1.14).

That is not to say that its predictions will *always* be in close agreement with experimental reality. Only for partly or wholly transparent layers between parallel uniform-temperature walls is that to be expected. But, although further research is needed, limited experience has shown that it never makes physically unreasonable predictions; and its computational expense is small.

So small is it indeed that IMMERSOL can be used when wavelength dependency is too great to be ignored. This arises, for example, when short-wavelength solar radiation provides a source of heat, that is, redistributed by way of long-wavelength low-temperature infrared radiation between the terrestrial objects on which it impinges. Thus, to use T_3 as the measure of the latter radiation and T_4 , say, as a measure of the former would be much more realistic than to ignore the wavelength dependence entirely, as is commonly done. To split the wavelength ranges into 10 or more bands would not significantly strain computer resources.

The author is, however, not aware of any practical exploitation of this possibility. As mentioned in the preceding text, radiative-transfer research is not very fashionable.

3.2. The wall-distance trick

3.2.1 How to calculate W_{gap}

The seriously interested reader of [Section 3.1](#) will have perceived a lacuna in the argument, for nothing has been said about how the vitally important W_{gap} quantity is to be calculated or indeed about what it *means* for spaces that are cluttered with solid objects of various shapes and sizes. A “data center,” that is, a large hall filled with computer cabinets and air-cooling equipment, is a case in point. Radiative heat transfer plays a significant part in lowering the temperature of the “hot spots,” in which the center manager must watch out for. But what meaning has W_{gap} in such a cluttered space?

There is an answer and again it has a somewhat “tricky” character: as does IMMERSOL itself, it produces answers that are exact in simple circumstances and never unreasonable in others. In order to whet the reader’s appetite, attention is drawn to three images (Figs. 1.29–1.31), the origin of which will be explained.

Let the task be to apply the IMMERSOL model for calculating the rate of radiative heat transfer between the two boxes of Fig. 1.29, the walls of which are held at different temperatures. The radiation will supposedly pass through the also empty duct that connects them, the walls of which will be supposed insulated. The emissivities of duct and box walls will be supposed known.

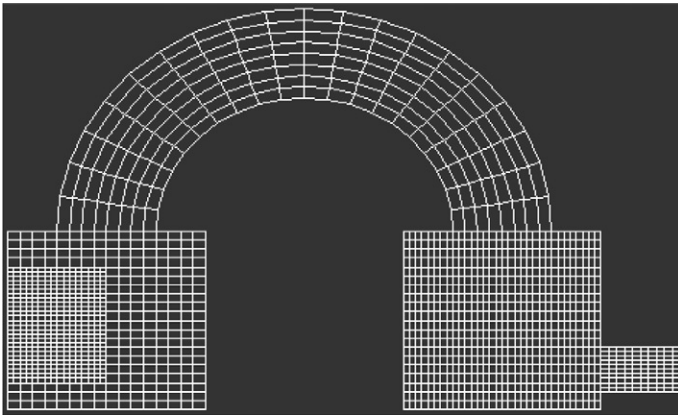


Figure 1.29 Computational grid for two boxes and a connecting duct.

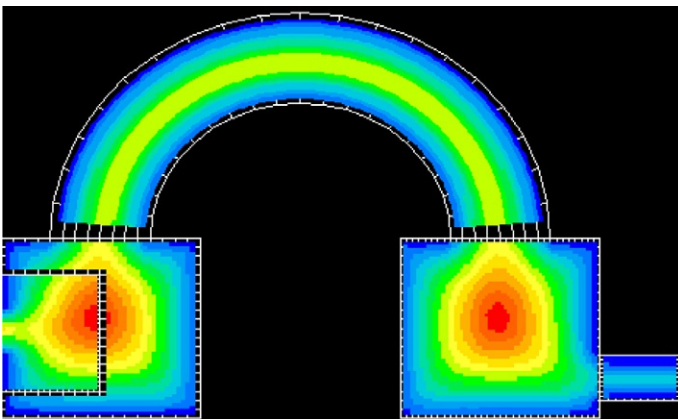


Figure 1.30 Computed contours of distance from a solid wall.

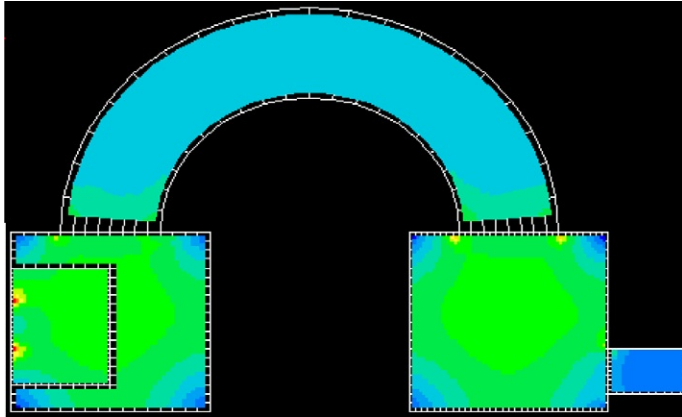


Figure 1.31 Computed contours of gap between walls.

Since IMMERSOL has reduced the task to the level of a heat-conduction one, it is easy; but it requires W_{gap} values to be known for every point in order that local conductivity can be computed.

Figure 1.30 shows the distribution not of W_{gap} but of a related quantity, W_{dis} , the distance of each point within the boxes or duct from the nearest solid wall. This is not a quantity that IMMERSOL uses; but it is calculated at the same time as W_{gap} .

Understandably, the lowest values are at the walls themselves; and the highest values are at the centers of the boxes. The corresponding values of W_{gap} appear in Fig. 1.31.

Equally understandable, W_{gap} appears to have a uniform value inside the connecting duct, for its walls are indeed parallel. Within the boxes, it is less uniform; but its highest value is about twice as large as that within the duct. These are plausible findings, the origins of which lie in the numerical solution of a Poisson equation now to be described.

3.2.2 The L equation

The trick that IMMERSOL has exploited comes from the turbulence modeling field. There, it is often desired to calculate the distance of a point in a fluid from the nearest solid wall; and a convenient way of doing so is to solve the following differential equation:

$$\text{div grad}L = -1 \quad (1.25)$$

with the boundary condition $L=0$, wherever solid is present. Since the original publication [40] is somewhat obscure, the idea that it expresses will be spelled out at length.

The equation is similar to that for temperature within a uniformly conducting medium, having a uniform heat source, and in contact with solids and other surfaces at which the temperature is held at zero. When it has been discretized and expressed in customary finite-volume form, it is easily solved by the linear equation solver of any CFD package, whether the geometry is 1D, 2D, or 3D.

The variable L is not itself the distance from the wall, even though it is proportional to that distance at locations very close to a wall. Its dimensions are indeed those of length-*squared*. However, the wall distance can be deduced from the solution for L , as can also a plausible estimate of the effective distance between walls. The method is to derive, by considering a simple geometry, namely, that between two parallel walls, relationships between

- the distance from the wall W_{dis} and
- the distance between walls W_{gap} , on the one hand, and
- the local value of L and
- the local value of its gradient, on the other

and thereafter to *presume* that the relationships have general validity.

3.2.3 The parallel-wall situation

Let the distance measured from one wall be γ , and the distance to the opposite wall γ_1 . Then the 1D form of Eq. (1.25), namely,

$$d^2L/d\gamma^2 = -1, \quad (1.26)$$

can be integrated to give

$$dL/d\gamma = -\gamma + A, \quad (1.27)$$

where A is a constant, and then further to give

$$L = -\gamma^2/2 + A\gamma + B, \quad (1.28)$$

where B is another constant.

Insertion of the boundary condition $L=0$ at $\gamma=0$ and $\gamma=\gamma_1$ yields

$$B=0, \quad \text{and} \quad A=\gamma_1/2$$

with the result

$$L = \gamma(\gamma_1 - \gamma)/2 \quad (1.29)$$

$$L' = \gamma_1/2 - \gamma \quad (1.30)$$

where L' stands for $dL/d\gamma$.

Elimination of γ_1 from the two equations yields

$$L = \gamma(L' + \gamma/2) \quad (1.31)$$

which is a quadratic equation, easily soluble for γ .

From its solution, follow with W_{dis} substituted for γ and W_{gap} for γ_1 :

$$W_{\text{dis}} = \left(L'^2 + 2L\right)^{1/2} - L' \quad (1.32)$$

$$W_{\text{gap}} = 2\left(L'^2 + 2L\right)^{1/2} \quad (1.33)$$

It is these equations that are employed generally, L and L' being obtained for each point in 2D or 3D space from the numerically computed solution of Eq. (1.25).

They have been found to give plausible results in all situations; but of course, neither W_{dis} nor W_{gap} has an unequivocal meaning when the walls exhibit corners, whether concave or convex.

It is interesting in this connection to consider a pipe of circular cross-section, for which it is again easy to obtain an analytical solution for L . The earlier-mentioned equations then show that the expression for W_{dis} is exactly correct in the immediate vicinity of the wall; and it rises to a maximum equal to radius divided by the *square root of 2* at the center of the pipe.

W_{gap} on the other hand varies between pipe radius times $2^{1/2}$ at the center to the radius times $2^{-1/2}$ near the pipe wall. One can therefore conclude that even extreme departures from the presumed parallel-plane conditions lead to not wholly implausible results.

3.2.4 Concluding remark

Before leaving the topic of wall-distance and wall-gap calculation, it is necessary to make clear that the L -equation method has no physical basis whatever. Its status is that of a “lucky guess,” its only justification being that “it works.” Those who are reluctant to use so dubious a trick should ask themselves: “What else can I do?”

3.3. The cut-link trick

3.3.1 Introduction

It has already been mentioned in [Section 3.1](#), under “Trends,” that grids of arbitrary polygonal cells are giving way in respect to popularity to variants of the “cut-cell” or “immersed boundary method” [53] kind. The present author has for several years been using one variant of the former, of which the details have never been fully published; moreover, he is at present in the process of developing a simpler but more powerful variant. It therefore accords with the purposes of this chapter to describe the first variant, to explain why it is now being superseded, and to record in more detail than is usual what the main features of the new variant actually are.

The first variant was called “PARSOL,” because it handled cell PARTIALLY filled with SOLID material. The new one is called “SPARSOL,” which stands for Structured PARSOL. Strictly speaking, both variants have some unstructured features, but SPARSOL has fewer than PARSOL, as will be explained. The main difference is that PARSOL was a true “cut-cell” technique in that rectangular cells, of which some *edges* were cut by the surfaces of solid bodies, were regarded as divided into *two* “subcells.” In general, these were of nonrectangular shape. Balance equations were formulated by treating both these subcells as control volumes. The number of equations to be solved therefore increased, which required somewhat troublesome changes in the solver.

SPARSOL, by contrast, considers cut *links* rather than cut *edges*, a link being the line joining two cell-center nodes. It therefore creates no new control volumes or corresponding equations; so the solver requires no change. What *it* does is to make such changes to the *coefficients* and perhaps also to the *source terms* of those equations as will best express the interactions between the fluid and the solid materials.

“*Best* express” is the phrase used, not “*perfectly* express”; and it is preferred advisedly. Perfection is never to be expected of a *finite*-volume (or *finite*-difference or *finite*-element) method. “Near enough” is all that can be hoped for; and if it is conjoined with simplicity, it is very good indeed.

3.3.2 The pros and cons of PARSOL

The major “pro” of PARSOL was of course that it removed entirely the grid-generation problem, which so troubled the arbitrary unstructured-grid users. Defendants of the latter practice argued that theirs was more accurate—and probably, they were right. But how great the difference in

accuracy was and whether it was worth the effort were never systematically put to the test. (Question to readers #3: Is the last statement true? And, if not, where can a systematic comparison be found?)

When first introduced, PARSOL was used only for hydrodynamics problems. Therefore, no finite-volume equation for the in-solid subcell had to be solved; and the only changes to the coefficients of the finite-volume equations were those that accounted for the reduced volume areas and distances of the in-fluid subcell when compared with the uncut whole cell. An account *was* taken of the size and orientation of the (often) inclined interface between the solid and the fluid; and the wall functions used in calculating the velocity components and turbulence quantities were duly modified. That pressure gradients were no longer aligned with velocity directions was not considered however; nor was the fact that sometimes the true thickness of the fluid boundary layer was *not*, as was tacitly presumed, much larger than the near-wall cell size.

It was when PARSOL started to be used for conjugate heat transfer problems that the in-solid subcells had to be used as supernumerary finite volumes. The changes made to the solver were at first excessively explicit, which entailed that the convergence of the temperature equation was sometimes inordinately slow. Later, more implicitness was built-in, with consequent increased speed of convergence, and still was added simultaneous solution for the radiosity temperature, that is, the T_3 of IMMERSOL.

This last addition increased the complexity of the solver, which occasionally led to divergence or at least to physically dubious solutions. It was while seeking to interpret and correct these deficiencies that it was recognized that it was the extra-control-volume feature that was the basic cause of the trouble, thence sprang the search for a better alternative, with SPARSOL as the result.

There was however an independent and even stronger reason for making the change, namely, that PARSOL could not cut its cells into more than two parts: one solid and one fluid. If it was to handle thin solid objects that cut the grid obliquely, only a very fine grid could be used; and this incurred serious computer-time penalties. SPARSOL is free from this crippling restriction.

3.3.3 Detecting the link intersections

3.3.3.1 The problem

Whether they are the cut edges of PARSOL or the cut links of SPARSOL, both procedures require intersections of lines with surfaces to be detected, their locations stored, and associated geometric quantities to be computed.

Detection can be done in more than one way. Having seen no discussion of this important matter in the literature, the author will provide one, based on his own experience.

First, it must be explained that the shapes of the surfaces of solid objects are always supplied in one of two ways: via *formulas* or via *facets*. The position, shape, and size of a sphere, for example, can be completely and compactly specified by the formula:

$$(x - x_0)^2 + (y - y_0)^2 + (z - z_0)^2 = r^2 \quad (1.34)$$

where x , y , and z are points on the surface; x_0 , y_0 , and z_0 are the Cartesian coordinates of the center; and r is the radius. Just four parameters will suffice. For such shapes, it is easy to determine the location of intersections of their surfaces with any straight line, whether an edge or a link, by way of algebra.

Far more often, however, the same sphere will be described by way of facets, as illustrated in Fig. 1.32, which shows a somewhat crudely faceted sphere within its bounding box. The information needed to describe it is voluminous, consisting mainly of the Cartesian coordinates of each facet vertex. The facet method is nevertheless often preferred for the use of formulas because it can be used for objects of *any* shape. A procedure must be therefore devised for determining the intersection, if it exists, of each facet with each grid line. Such a procedure will be described; it can be used for two- or 3D Cartesian or cylindrical-polar grids, whether structured or unstructured. Extension to body-fitted grids is also feasible.

3.3.3.2 The 2D projection method (2DPM)

In this, the first-used method, now superseded, the facets of the object were projected on to a plane normal to one of the coordinate directions, as triangles or quadrilaterals.

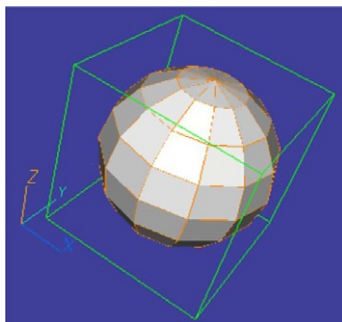


Figure 1.32 Facetted sphere.

Cell edges appeared in the projection plane as points, and the existence of an intersection was evidenced by the cell-edge point lying within the projected facet area. This was detected by calculating the areas of triangles having facet-edge projections as base and the grid-line projection as apex. The determination of whether the grid-line projection lay inside or outside the facet projection depended on the signs of these areas. Thereafter, the normal-to-plane location of the intersection could be calculated, and the geometric properties of the cut-cell computed and stored for use.

The disadvantages were the slowness of the area calculation, the hit-or-miss nature of the decision as to whether points lay inside or outside, and the obscurity of the intersection calculation. Moreover, as implemented, no advantage was taken of the economies that can be made when the flow situation to be simulated is two- rather than 3D. The 2DPM coding was thus found, after intensive study, to have several drawbacks, of which the most serious were as follows:

- It could not be relied upon always to detect intersections between facets and cell edges, because of the lack of control of “tolerances,” that is, the differences of distance between what was and what was not an intersection.
- It could not directly treat the commonly occurring 2D flow situations, but had to convert them into pseudo-3D ones, which was at best uneconomical and at worst contributed to the “missed-intersection” phenomenon.
- Even when intersections were correctly detected and their positions computed, the excessive amount of computation involved imposed a serious delay on the start-up of the true CFD calculations. This was the most serious of the three.

3.3.3.3 The 2D section method (2DSM)

It was for these reasons that the now-preferred 2D *section* method was invented. It is so named because it finds first the *straight-line segment* that a facet makes *if* it intersects one of the planes containing cell edges (for PARSOL) *or cell centers* (for SPARSOL). Then, it seeks intersection *points* that the segment may make with the grid lines corresponding to the two other coordinate directions. [Figure 1.33](#) illustrates this.

The procedure is as follows:

- Choose a first constant-grid coordinate plane. If the grid is cylindrical-polar, of course, the grid coordinate cannot be the radius, for that is not a plane. Then, lines corresponding to the not-chosen grid coordinates can be imagined as inscribed on the chosen plane either as straight lines or (in the cylindrical-polar case) as circles.

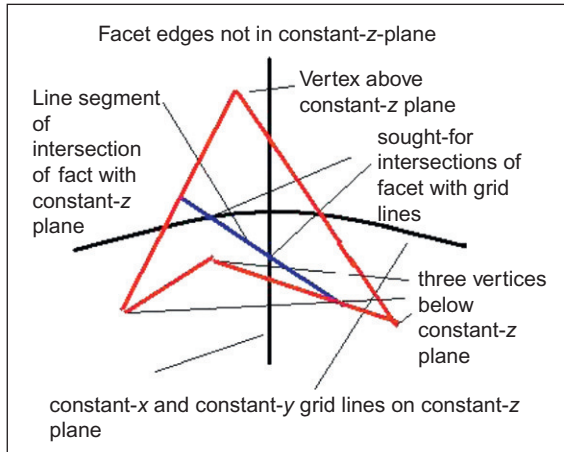


Figure 1.33 Illustrating the 2DSM.

- Check the coordinates of the vertices of the facet to determine whether they all have equal values of the normal-to-plane coordinate. If they do, no intersections can exist, so the facet can be discarded; otherwise, proceed as follows.
- Examine each edge of the facet in turn and consider the coordinates of the vertices at each of its ends. If the normal-to-plane values of all of these are less than that of the plane or all of them exceed that value, no intersection is possible so the facet can be discarded; otherwise, proceed as follows.
- For each pair of vertices lying on opposite signs of the chosen plane, calculate the in-plane coordinates of the location of the vertex-joining edge with the chosen plane. This lies at one end of a facet-with-plane intersection *segment*.
- By comparison of the coordinates of these pairs with the coordinates of the “inscribed” grid lines, determine whether the segment intersects one or more of these. If not, discard the facet; otherwise, proceed as follows.
- Use the appropriate algebraic expression, quadratic, or linear according to whether the coordinate in question is or is not the radius, to calculate the coordinates of the intersection point.
- Unless the problem is 3D rather than 2D, choose a *second* constant-coordinate plane and repeat the process, with one difference: it is necessary, having found a facet-plane intersection segment, to seek its intersections only with the grid lines corresponding to those of the first chosen *plane*. The reason is that intersections with other grid lines have already been found.

- The final step is to record which part of the intersected grid lies inside the object by making use of the convention connecting the order of listing of the facet vertices with the side of the facet on which the object itself lies.
- When this has been done for all the facets of the current object, repeat the process for the next object and continue thus until all the objects have been dealt with.

3.3.3.4 Other aspects of facet-grid-line intersection detection

The just-described 2DSM works well when it is presented with a well-ordered set of objects and associated facets. However, architects and others often present, as objects around which they require flow to be computed, collections of facets, produced by Computer-Aided-Design packages, which are far from being well ordered. From the *architect's* viewpoint, they are satisfactory, for the buildings and other objects have the right *visual appearance*, but commonly encountered defects are the following:

- Adjacent facets may bear conflicting information about which side is “in” and which side is “out.”
- Some facets are absent, so that the surface of a solid object appears to have holes in it.
- Some needless facets are supplied, having identical vertex coordinates (listed but in a different order), for example, those representing the floor of one room and the ceiling of the room below it, when the flow in neither room has to be computed.
- Far too many facets are supplied, for example, those representing the individual steps in a staircase, for the computational grid to be take account of.

It is desirable therefore to pass such CAD-package output through a *facet-fixing* program before it is delivered to the CFD code; but even after this, some difficulties may be encountered. Specifically, the facets supplied may show that some of the objects *overlap*, in the sense that two or more objects lay claim to the same locations in space. Alternatively, two objects may *touch*, in the sense that their facets both intersect the same grid line at the same location, but from opposite sides. These problems will be discussed in SPARSOL terms, which is to say that the grid lines in question will be internode links rather than cell edges.

The “overlapping” problem can be solved by imposing the rule “last claimant wins.” There can be only one material at any particular grid node, for example; and the “last-prevails” principle allows material settings to be made without inquiry as to whether a previous one has been made at the node in question.

The “touching” problem can be solved by the same rule. All that is necessary is to arrange that no decisions about the magnitudes of internode coefficients are made until all material settings have been completed.

One final problem should be mentioned: a link between grid nodes can be cut twice by facets belonging to the same body. This can occur when the thickness of an object is small compared with internode distances. In such circumstances, it might be said that the grid ought to be refined, but with structured Cartesian or cylindrical-polar grids, the needed refinement near the body results in *not*-needed refinement elsewhere. The more economical solution is to move one of the nearby grid nodes so that it lies within the object; then, one of the two intersections moves from the cut internode link to another, which was not previously cut. Thus, the double-cut difficulty is removed. But this is just one aspect of geometry adjustment, discussed in the succeeding text.

The overlapping, touching, and double-cutting problems are not confined to objects that are defined by facets; they can arise also with objects defined by formulas. After the intersections have been found, it is immaterial which method was used to define the shapes.

3.3.4 Changing coefficients in SPARSOL

3.3.4.1 The problem

The coefficients connecting the solved-for variables at neighboring grid nodes typically represent the influences of diffusion (laminar and turbulent) and convection. In the immediate vicinity of a solid surface, it is usually the former influence that predominates; therefore, the present discussion will consider diffusive influences exclusively. Moreover, for concreteness, the dependent variable considered will be temperature; and a single phase will be supposed present at each grid node. The material property in question is thus the thermal conductivity, λ .

The commonly used formula for the heat transfer coefficient, C_{LM} , between points L and M in Fig. 1.34 is, because all the material between the points is solid,

$$C_{LM} = \lambda_{\text{solid}} A / (x_M - x_L) \quad (1.35)$$

wherein x denotes the horizontal position and A is the surface area of the face between the cells. That for C_{MR} , on the other hand, is

$$C_{MR} = A / \{ (x_{MR} - x_M) / \lambda_{\text{solid}} + (x_R - x_{MR}) / \lambda_{\text{fluid}} \} \quad (1.36)$$

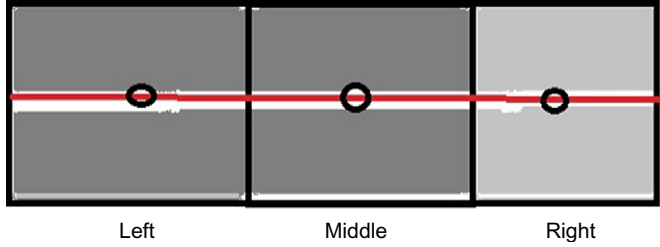


Figure 1.34 Cells wholly filled with solid (darker) or fluid (lighter).

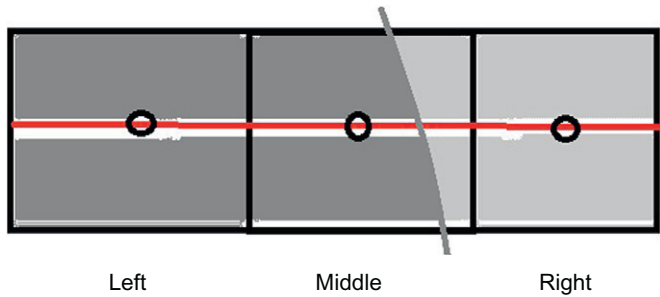


Figure 1.35 Solid object cuts link MR in nonstandard position.

wherein x_{MR} denotes the horizontal position of the interface between M and R. This has the value $W_M/2$, where W_M is the horizontal width of cell M.

3.3.4.2 Changing the distances

Consider now the situation in [Fig. 1.35](#).

The equation to fit this situation is obviously

$$C_{MR} = A / \{ (x'_{MR} - x_M) / \lambda_{\text{solid}} + (x_R - x'_{MR}) / \lambda_{\text{fluid}} \} \quad (1.37)$$

wherein x'_{MR} now denotes the horizontal position of the location at which the object surface cuts the internodal link MR. This location is known as a consequence of the operations described in [Section 3.3.4.1](#). Therefore, two actions to be taken after finding the intersections are first to determine which nodes lie in the solid and second to recalculate the distances from the nodes to the interfaces.

A major defect of PARSOL was its inability to handle thin objects. How SPARSOL deals with them is shown in [Fig. 1.36](#).

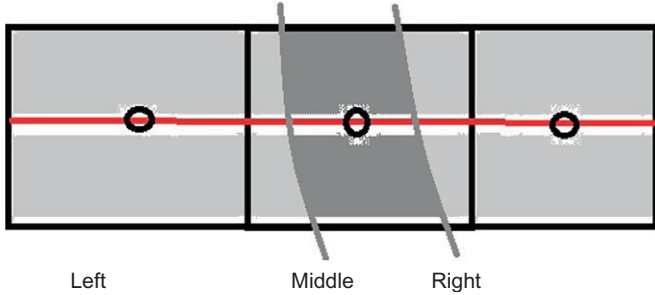


Figure 1.36 Thin object cuts two neighboring links.

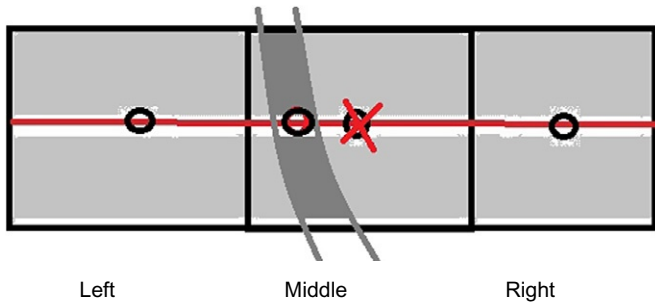


Figure 1.37 Thin object cuts one link.

Figure 1.36 differs from Fig. 1.35 in that link LM is intersected and link MR. This simply entails that the equation

$$C_{LM} = A / \left\{ (x'_{LM} - x_L) / \lambda_{\text{fluid}} + (x_M - x'_{LM}) / \lambda_{\text{solid}} \right\} \quad (1.38)$$

must be used also, the quantity x'_{LM} being modified from its standard value.

What if the two surfaces of the thin body cut the *same* internode link as shown in Fig. 1.37?

More than one strategy could be chosen; but the one here illustrated is move the node. The equations are therefore

$$C_{MR} = A / \left\{ (x'_{MR} - x'_M) / \lambda_{\text{solid}} + (x_R - x'_{MR}) / \lambda_{\text{fluid}} \right\} \quad (1.39)$$

and

$$C_{LM} = A / \left\{ (x'_{LM} - x_L) / \lambda_{\text{fluid}} + (x'_M - x'_{LM}) / \lambda_{\text{solid}} \right\} \quad (1.40)$$

wherein x'_M replaces x_M . This is all that needs to be said.

3.3.4.3 Changing the areas

It is, however, not only the distances that require to be changed in order to express the influence of nonstandard intersections of internode links. Consider, for example, the situation illustrated in Fig. 1.38.

Earlier, the intersected horizontal (red) links were considered; but attention is now turned to the nearby not-intersected vertical (green) links; and the question is: how should these be modified so as to account for the nonstandard locations of the red-link intersections? The answer is obvious: by way of the *areas* in the coefficient formulas. Obviously, the coefficient between the LowLeft and HighLeft nodes, for which λ_{fluid} is the correct conductivity, is associated with a *less-than-standard* area.

Correspondingly, the coefficient between LowRight and HighRight, for which λ_{solid} is the correct conductivity, is associated with a *greater-than-standard* area.

These area changes can be deduced from the red-link-intersection locations resulting from the actions described in Section 3.3.4. How? By linear interpolation. Are there interpolation formulas that will take into account the putative curvature of the object surface also? “No” is the answer, to which might be added: “Of course not. Do not expect too much. If you want more accuracy, use a finer grid.”

In the previously mentioned examples, it has been only the red links that have been intersected. What should be done if only the green links had been intersected is obvious: y -distances should be changed rather than x -distances; but what should be done if both are intersected as illustrated in Fig. 1.39.

The safest answer to this question is to do nothing special at all. The LowLeft-to-LowRight and LowRight to HighRight links are not

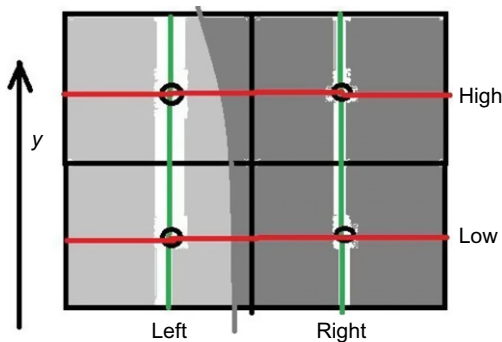


Figure 1.38 How intersected links influence areas.

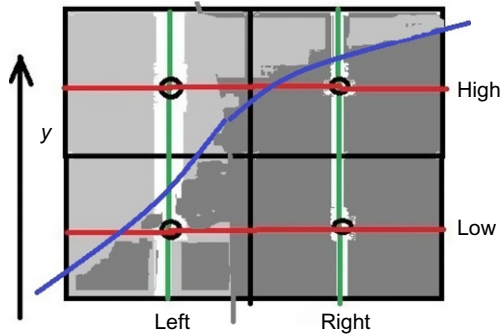


Figure 1.39 Nodes with two links.

intersected; but they do have slightly reduced areas. The other links are singly intersected; so they should have their coefficients computed from Eqs. (1.39) and (1.40). More complex rules could be thought of; but it is better to accept the “do not expect too much” advice.

3.3.4.4 Adding fluid-side resistances

It was mentioned in the preceding text that if the flow is turbulent, the thermal conductivity to be used is the sum of the laminar and turbulent values. However, close to walls, the turbulent contribution varies steeply with distance from the wall; and with structured grids of economically tolerable fineness, this often means that the only way to determine an appropriate “effective” value is by use of a “wall function.” No difference in principle arises when links are cut by the surface of bodies at nonstandard locations; but of course, the changed distances have to be taken into account.

3.3.5 Modifying sources

Source terms, in balance equations for mass, momentum, energy, and chemical species, are often proportional to the volume of the cell or more precisely to the volumes of each of the materials within the cell. The same is true of the terms representing variations with time when an unsteady-state computation is in progress.

PARSOL modified the volumes associated with cut cells, diminishing these by the amount that was ascribed to the “subcells” that it created. SPARSOL also modifies volumes associated with each of its nodes. Since the number of these nodes remains constant, some of its volumes are diminished and others increased. The magnitudes of these changes are computed

from the link–intersection locations in straightforward ways, too obvious to be spelled out here.

Momentum sources play a *special role*, for the presence of solids within the fluid commonly forces the velocity at nodes within them to have the value prescribed or calculated for the object. In SPARSOL, these are best specified by way of cell–wise linearized sources, thus

$$v_source = large_number(v_object - v_local)$$

This has the result of introducing such a large momentum source, if the local velocity differs at all from the object velocity that v_local is forced to equal that velocity very closely. Very often, the object is not moving, so that v_object equals zero, as is shown in Fig. 1.40, where SPARSOL is being used to represent the flow deflection caused by an airfoil at a high angle of incidence.

Of course, with such a coarse grid, the velocity distribution close to the airfoil surface cannot be well represented; therefore, the calculated frictional force on the object will be very far from correct. This is the reason why those concerned with the simulation of flows around aircraft, for which the frictional component of drag is very significant, often go to great trouble in order to place finely divided cells in the boundary–layer region. Figure 1.41 illustrates this trend.

The computational expense is very great. Therefore, two remarks are worth making:

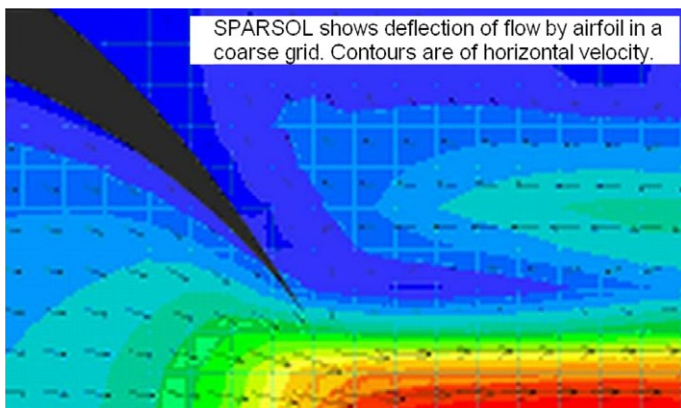


Figure 1.40 SPARSOL's use of momentum sources to represent an airfoil.

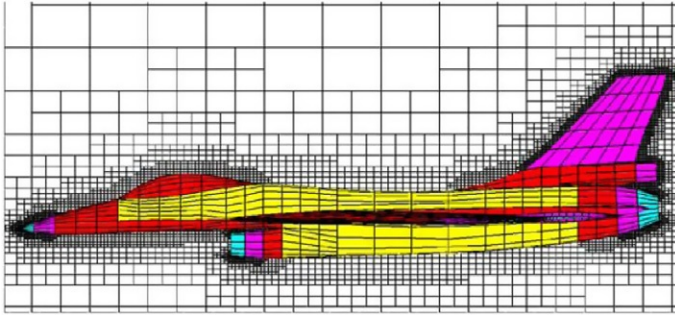


Figure 1.41 Unstructured-grid refinement near-solid surface.

- First, it is improbable that the grid is *ever* made fine enough for numerical accuracy, for turbulence models require energy sources to be computed and these depend upon the squares of velocity gradients. Very fine grids are needed if these are to be accurate.
- Second, there is a much simpler and cheaper way of achieving the required fineness. It is to calculate only the pressure distributions in the air just outside the boundary layer by means of a 3D *elliptic-flow* solver (which may even be of the highly economical potential-flow kind). Then flow within the boundary layer can be calculated on as fine a grid as necessary by a *parabolic-flow* solver.

The second feature may, like IMMERSOL, LTLS, and SPARSOL, also be regarded as a “trick,” additionally “unfair” because it robs the heavy-weight-computing enthusiast of the excuse for demanding ever more number-crunching power. Yet, the argument in its favor is compelling. The essential characteristic of boundary layers is that they have one *predominant direction of flow*. Then, if the mathematical solution procedure itself “goes with the flow,” 3D problems can be solved with a 2D grid; and one does not need much memory for that.

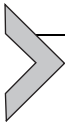
Of course, the 3D and 2D calculations have to be linked. The parabolic solver has to report to the elliptic one the “displacement-thickness” distribution over the aircraft’s surface, in order that the elliptic solver can modify its first guess, which may have been to assume that the thickness was zero everywhere. So back-and-forth iteration is necessary. But it is not to be expected that *many* iterations will be needed; unless, that is, the conditions are close to those leading to boundary-layer separation. Aircraft-safety rules preclude that, in any case.

The idea of coupling potential-flow with boundary-layer calculations is far from new; and a fairly recent NASA “2D-airfoil-challenge” exercise [37]

showed that its accuracy is comparable with that achievable by all-elliptic 3D Reynolds-averaged Navier–Stokes solvers. But there, the boundary-layer methods employed were all of the preCFD integral-equation kind; and these are restricted to 2D. No one seems to have thought of using *numerical* parabolic solvers, which, of course, are not so restricted. Was not, after all, the now-widely used SIMPLE algorithm [5] first introduced for 3D boundary-layer calculations?

3.3.6 Concluding remarks about SPARSOL

SPARSOL, as just described, is simply a variant of what has come to be known as the immersed boundary method. Whether it is superior or inferior to others can be determined only by extensive tests that are beyond the present author's competence. All that can perhaps be claimed is that, because of the publisher's generous space allocation, it is at least the most completely described. (Question to readers #4: is this true?)



4. TRY-ONS

4.1. A differential equation for mixing length

4.1.1 What ludwig prandtl might have done

Prandtl was nearing the end of his life when he published his one-equation turbulence model in 1945; so perhaps he did not have time to recognize that a more advantageous dependent variable than k might have been chosen. Since his time, other choices have been made, in particular that of Nee and Kovasny [41] in 1968.

The novelty introduced by them was the proposal that the effective viscosity, ν_{eff} , as well as appearing as a coefficient in the diffusion terms, should *itself* appear as the dependent variable of the differential equation. And why not? If Harlow and Kolmogorov could treat dissipation rate, ε , and frequency, f , as conserved properties, why not ν_{eff} as well?

Had Ludwig Prandtl followed the same line of thought, then the k -equation would not been needed. He might well have chosen his *mixing length* as the conserved property; then the “*mixing length transport model*” might be among those used by engineers today.

4.1.2 The spalart–allmaras viscosity-transport model

Before speculating further about what Prandtl might have done, it should be mentioned that, long after it had become widely accepted that only turbulence models with two or more differential equations were worthy of study,

the Nee–Kovasny innovation was revived and developed by Spalart and Allmaras [42, 43]. Their one-equation model has been shown often to perform and more sophisticated ones, at least in the aeronautics-related problems for which it has been tested. Extensions to supersonic flow have been successfully made [44].

Inspection of the now-extensive literature on the subject has evoked the following thoughts in the present author's mind:

- Spalart's remark in Ref. [44], "turbulence modeling *can* stagnate," is a wise warning, which he at least is heeding.
- Also notable is his remark: "No deep reason was seen why two equations were indispensable, although this remains a widespread position."
- He has also felt free to formulate his one equation in unconventional ways, using vorticity rather than strain rate in source terms and allowing the turbulent-diffusion terms to conserve not v_{eff} but $v_{\text{eff}}^{1.62}$.
- It is with such a free-from-preconception attitude that any alternative one-equation model should be considered.

4.1.3 The "mixing length transport try-on"

Much is known about the distributions of mixing length in turbulent flows, including that, at high Reynolds numbers, it increases with flow-direction distance x , raised to a power, equal to

- unity, in a plane mixing layer, a plane jet, or a circular-section jet, each having its own proportionality constant;
- one-half in a plane wake, for example, behind a circular cylinder; and
- one-third in an axisymmetric wake, for example, behind a sphere.

Moreover, it tends to be 0.41 times the distance from the wall, as a solid wall is approached; and downstream of a grid of parallel rods, it tends to be 0.103 times the distance between the rods [45]. Within a long pipe of circular cross-section, it obeys the Nikuradze [46] formula:

$$l_m/R = 0.14 - 0.08(1 - \gamma/R)^2 - 0.06(1 - \gamma/R)^4 \quad (1.41)$$

where γ is the distance from the wall and R is the pipe radius.

In the semilaminar region very close to a wall, the formula of van Driest [47] is believed to prevail. It is

$$l_m/\gamma = 0.41 \{1 - \exp(-\gamma^+/26.0)\} \quad (1.42)$$

All this constitutes perhaps a richer body of empirical information than the v_{eff} transport modelers start from.

The task is to devise a differential equation of the form

$$\partial(\rho l_m)/\partial t + \text{div}(\rho_1 \mathbf{v}_{i,j} l_m) = \text{div}(\Gamma \text{grad} l_m) + S \quad (1.43)$$

which, when solved numerically, will yield mixing length distributions that accord with these simple-situation findings; then, it can be reasonably hoped, the solutions to the equations with different boundary conditions will also fit experimental findings reasonably well.

The crucial question is: how should the source-and-sink term, S , be expressed in terms of velocities and other variables, so as best to fit the data? A reasonable first guess for high Reynolds numbers would be

$$S = \text{const1} * \text{strain_rate} * (l_m - 0.41 * W_{\text{dis}} - 1.03 * \text{profile_width}) \quad (1.44)$$

wherein

- l_m is the local mixing length, to be used with Eq. (1.1);
- const1 is a dimensionless constant or a function of dimensionless properties of the local flow, chosen so as to fit known experimental data regarding mixing length distributions, such as those cited earlier;
- strain_rate would be deduced from local velocity gradients in a conventional manner;
- W_{dis} is distance from the wall computed by way of the “thick” of Section 3.2; and
- profile_width would be introduced so as to reflect the influence of such geometric factors as the spacing of the rods in an upstream grid.

Equations (1.42) and (1.43) are *only* first guesses; and a combination of physical intuition and numerical resourcefulness will be needed to translate them into finite-volume equations and convergent solution procedures. For example, at the upstream edge of an ideal mixing layer, the strain rate is infinite and l_m is zero; for the furthest upstream control volume, an approximation must be employed for their finite product that makes physical sense.

4.1.4 How “const1” might be determined: the “reverse-engineering” approach

Publications about turbulence models commonly report what empirical auxiliary functions are to be used, but not how they were arrived at. In the present case, those functions have not yet been determined; so it is proper to propose how they *could* be. The approach suggested is here called “reverse engineering,” for it starts with given facts and tries to work out how they came about.

The facts to start with are the experimentally determined velocity profiles. For the simple situations listed in the preceding text, these can be approximately represented as piecewise polynomials. Then, the “reverse engineering” starts by *imposing* the corresponding velocities, if one’s CFD code allows it, at the corresponding nodes of the computational grid, by supplying linearized momentum sources to the cells surrounding them.

Thus, if the source is specified as, say, $1 \times e^6 (u_{\text{experimental}} - u)$, it will be large enough to make the calculated velocity differ little from the experimental one; and its magnitude, if printed out, will provide significant Information. Thus, if the effective viscosity of the computer code has been set equal to zero, the printed-out sources disclose magnitudes of the shear stresses that are present in the real flow.

The next move is to calculate, from the printed-out source differences, what are the shear forces at the boundaries of the velocity cells. This can be done by working from the free-stream boundaries of the layer, where the sources are zero, toward the center. From the shear forces and the known velocity differences, the effective viscosities for each internode link can be computed. If the code permits the link-by-link insertion of effective viscosities, doing this and observing whether the printed-out sources indeed now become small, is a useful test of the accuracy with which the whole operation has been conducted.

Once the effective viscosities are known, the corresponding mixing lengths for each link can be computed. Then, *solution* for l_m can be activated, the just-computed “experimental” values being fixed by linearized-source terms, in the same way as was done for velocity. The then-printed-out l_m sources provide information about the cell-by-cell values of the *whole* of the right-hand side of Eq. (1.43), that is, the contributions of both the S and the Γ terms. Disentangling the two contributions will involve (cautiously) making some presumptions.

Fortunately, not one but several simple situations exist to which this “reverse-engineering” process can be applied; and the relative importance of the S and the Γ terms is unlikely to be the same in each. Therefore, disentanglement may not prove to be too difficult. PhD students indeed are likely to relish the challenge.

In addition to the simple situations already cited, there exist others for which reliable data are available. The “backward-facing-step” is one that has been used for the critical assessment of two-equation models [48]. It is of interest because it exhibits free-shear-layer *and* near-wall *and* 2D recirculation effects. Whether the one-equation “mixing length transport

model” could handle all three simultaneously is a question of great interest. The Spalart–Allmaras model does *not* appear to have been tested for this flow.

4.1.5 Concluding remarks about mixing length transport

The purpose of the foregoing paragraphs is not to persuade readers that l_m is a better dependent variable to use than v_{eff} or k , but merely that it *might* be, and that nobody knows. Not only *can* turbulence modeling research stagnate, but also it *has stagnated*. It is hoped that some readers of this chapter will see and seize some of the many opportunities for further progress that still exist.

4.2. The population approach to swirling flow

4.2.1 The problem

Swirling turbulent flows are of great practical importance. They are employed

- in gas–turbine combustors in order to promote mixing of fuel and air and thereby to increase thrust per unit volume and combustion efficiency;
- in the large mechanically stirred reactors of chemical industry for similar purposes;
- in hydro- and aerodynamic cyclones in order to promote *unmixing*, that is, the preferential separation of elements of the mixture experiencing different body forces.

Such flows are also regarded as of such scientific interest that special conferences of theoreticians are devoted to them. Perusal of their proceedings, however, reveals an astonishing fact, namely, that although the preferential-separation process experienced by materials *carried by* the swirling flow is considered that the *turbulence itself* is subject to preferential separation receives no direct attention. Instead, attempts are made to “tweak” the constants and functions of turbulence models of the kind that are used for *nonswirling* flows, but with meager success.

4.2.2 A “try-on” solution

In a recent unpublished presentation at such a conference, [55] to which he now seeks to give wider publicity, the author proposed that the analogy with two-phase flows should be exploited. Figure 1.42 illustrates how a stream comprising a uniform mixture of water droplets of water suspended in vapor-phase steam behaves when it flows through a curved duct. The flow is from bottom to top. The colored contours denote volume fractions, yellow signifying “high” and light blue “low.”

Clearly, and understandably, the greater centrifugal forces on the droplets have caused the water to migrate to the larger-radius region, forcing the air to move to the inside of the bend. The point of the demonstration was to argue that, if the force differential had been caused by differences of *velocity* rather than of density, the effect would qualitatively have been the same.

In connection with Fig. 1.20, it was seen that the use of a two-member population of a single-phase mixture, when Navier–Stokes equations are solved for each of the members, can simulate qualitatively the transition from deflagration to detonation. May it not be therefore that the same model could at least throw some light on the “velocity-sifting” phenomenon that gives swirling turbulent flows their special character? And that a multi-member model might do still more?

For multimember populations, to solve Navier–Stokes equation sets for each member would be excessively costly; and it would be disproportionate in view of the guesswork that would be needed concerning the friction forces opposing the sifting process. Nevertheless, first steps with such guesswork applied to a 17-member model were reported in the just-mentioned presentation, the application being to an imaginary flow in the space between concentric cylinders, rotating about their common axis at different velocities, as shown in Fig. 1.43.

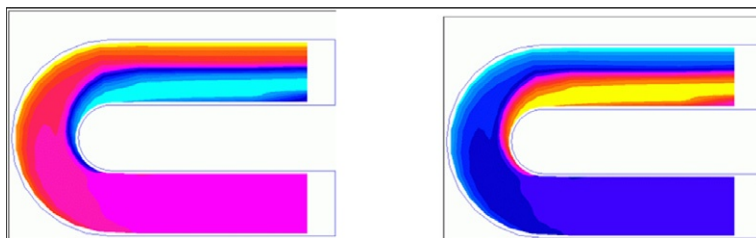


Figure 1.42 Computed volume fractions of water (left) and steam (right).

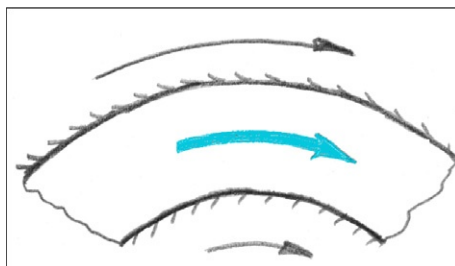


Figure 1.43 Flow between rotating coaxial cylinders.

It was postulated that at some entrance plane, on the left, the velocity population was extremely orderly, each member being located at the radius that corresponded to a linear velocity distribution from inner to outer radius. Turbulent mixing was then postulated as occurring, with a diffusivity corresponding to experimental data in fully developed plane channel flow. The consequent intermingling of the members was then computed.

The contour diagrams in Fig. 1.44 were computed for cylinders of infinite radius, that is, for *no* curvature. They showed for 3 of the 17 fluids how turbulent mixing causes the mass fractions to spread with distance downstream. This diffusion process is opposed by the collision/engulfment process that tends to even out the local probability density functions; and the fact that the contour lines become horizontal on the right indicates that the two opposing phenomena finally balance (Fig. 1.45).

Thereafter, calculations were carried out with finite radius, and in order to throw light on the role of the centrifugal forces, two cases were considered. In the first, it was the larger-diameter cylinder that had the higher velocity; in the second, it was the smaller-diameter one. One would expect the first to diminish the intermingling effect and the second to increase it. This expectation is borne out by the corresponding fluid-population distributions shown in Figs. 1.46 and 1.47, respectively.

The calculations just described were made to show that a multimember population, with longitudinal velocity as the population-distinguishing attribute, could be made at little expense and that the results are qualitatively plausible. The exercise was of the “try-on” character; and the conclusion no more than: “Yes, I think it might work.”

Perhaps that is more or less what Ludwig Prandtl thought after his first experiments with the mixing length model.

4.3. Hybrid CFD “Try-on”

4.3.1 The general idea

The word “hybrid” is often used nowadays in the turbulence modeling literature to describe the practice of employing different models of turbulence in different parts of the same field of flow. An example is the use of a steady-state RANS model close to a wall and an unsteady-state LES one elsewhere [49]. The “try-on” now to be proposed can be regarded as an extension of the idea: it involves using not only different formulations of the governing equations in the different regions but also different methods for solving them.

The idea is of course not new: and it was in common use by aerodynamicists long before CFD existed. Even then, aerodynamicists could predict

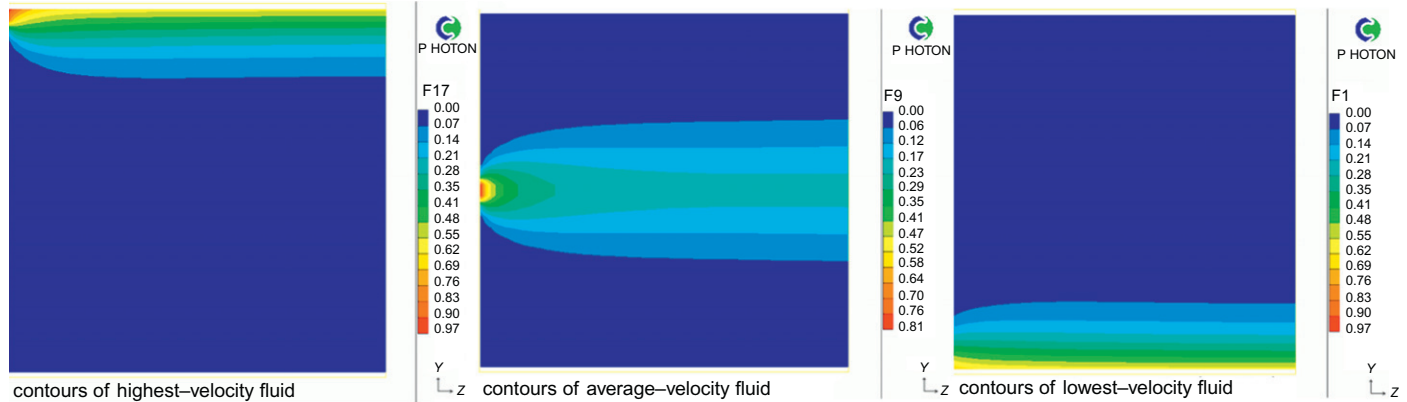


Figure 1.44 Contour diagrams of mass fractions of highest-, middle-, and lowest-velocity fluids, with flow from left to right and radius vertically upward.

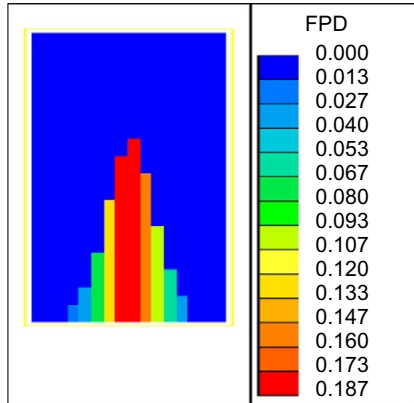


Figure 1.45 Computed fluid-population distribution far downstream for a location midway between the moving surfaces, for the case of zero curvature. Fluid 9, the middle-velocity population member, has the highest mass fraction, namely, 0.187.

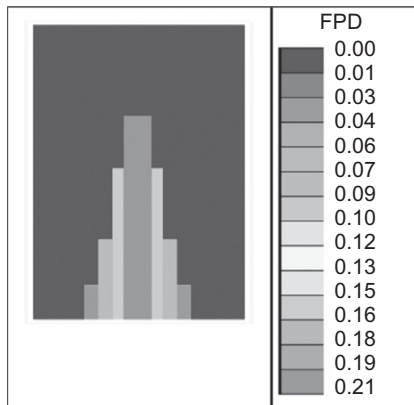


Figure 1.46 Computed fluid-population distribution far downstream for a location midway between the moving surfaces, for the case of faster-moving outer cylinder. Fluid 9, the middle-velocity population member, still has the highest mass fraction, and it has risen to 0.21.

their lift and drag. They used a combination of *potential-flow* theory with *boundary-layer* theory, proceeding iteratively:

- First source–sink distributions were sought that caused streamlines to coincide with the shape of the airplane. This led to distributions of *pressure* over the surface.

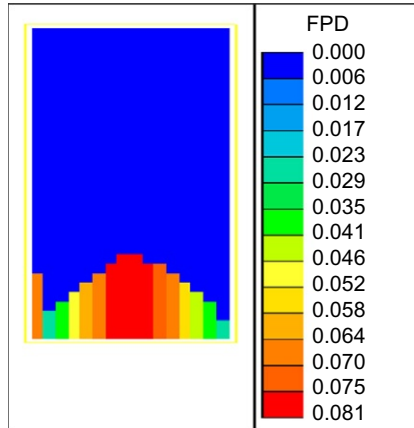


Figure 1.47 Computed fluid-population distribution far downstream for a location midway between the moving surfaces, for the case of faster-moving inner cylinder. Fluid 9, the middle-velocity population member, still has the highest mass fraction; but it has fallen to 0.081.

- Then, they used boundary-layer theory to calculate the “displacement thickness” of the layer, that is, the extent to which the airplane was bigger than at first supposed.
- Then, they repeated the first step with a new specification of airplane shape; and the second with the consequentially new pressure distribution.
- And so on until the changes of displacement-thickness distribution became small enough to ignore.

Of course, the boundary-layer theory was primitive, being of the 2D integral-profile kind. However, the principle was sound, and it still is. A recent application of the method to a 2D airfoil was referred to in Section 3.3.5; and the accompanying remarks will now be expanded upon.

4.3.2 The partially parabolic method extended

When, at Imperial College in the 1970s, the SIMPLE method, having been invented for 3D parabolic-flow problems, was recognized as applicable to elliptic problems also, both 2D and 3D, it was the latter that attracted the most attention. However, computers were still small, and any memory-saving device was welcome. One such device was the so-called partially parabolic method [50–52]; and the efficacy of the method was demonstrated by reference to turbulent flows in curved ducts and around the sterns of

seagoing vessels. This exploited the fact that, the downstream-to-upstream terms in the momentum equations being negligible, the equations became parabolic in nature; so they could be solved, once the pressure distribution was known, by the marching-integration procedure of Ref. [5], which required only 2D storage. Only the mass conservation equation, from which the pressure was computed, exhibited significant downstream-to-upstream influences; so it alone required a 3D grid.

The method attracted no attention outside Imperial College; and the present author's interests became deflected in the direction of two-phase flows in nuclear steam generators and in gas-turbine combustion chambers. To neither of these was the partially parabolic method applicable, for they exhibited no predominant direction of flow. Easily achievable developments were therefore not then pursued; but three such advantageous developments will now be outlined, as follows:

1. In the all the work carried out in the 1970s, the *same* grid was used for the pressure as for the other variables; but there was no need for this, and advantage in respect to realism could have been attained by using much finer cells in the parabolic grid than in the elliptic one. This is affordable, because the parabolic grid requires only 2D storage.

To allow for differences in the main flow-direction step sizes, the pressure gradients used in the momentum equation would have to be interpolated; but, since pressure varies much more gradually than other variables, little diminution of accuracy is to be expected.

2. In the early work, the volumes of space traversed by the elliptic and the parabolic calculations were also the same; but in the applications envisaged in the present "try-on," which include flows around aircraft and missiles, the parabolic calculation would be confined to the regions in which velocity gradients were significant, namely, close to the wall, and in the jets and wakes; for elsewhere, the flow is inviscid. This would generate further economies.
3. There would also be no need to have only one parabolic grid. Indeed as exchanges of information between elliptic and parabolic solutions proceeded, the stagnation point on the airplane nose might well shift from iteration to iteration. So a different parabolic grid would be needed each time. But why not? Grid generation for parabolic flows is very easy. Moreover, it is probable that *several* parabolic grids would be better than one; and the upstream boundary condition for farther-downstream ones would be reduced by interpolation in the values at the outlet surfaces of upstream ones.

It remains to ask: Why is this hybrid “mix-and-match” method not used? Are the advantages of economy and realism here envisaged not worth having? Or not recognized? Or recognized, but deemed illusory? Or is it that the possibility of solving 3D boundary-layer equations numerically is not widely understood?

4.3.3 Simulating automobile aerodynamics

Early CFD calculations of flow around automobiles made by the present author used computational grids such as that in Fig. 1.48. They extended over a much larger volume than that occupied by the vehicle; and, despite the fact that in the greater part of the volume the flow was inviscid, the 3D Navier–Stokes equations were solved throughout (Fig. 1.49).

It was a foolish practice of course; but even now, it is customary to employ a single grid, albeit of unstructured form. Therefore, it appears reasonable to ask: Why not use instead

- a 3D elliptic potential-flow solver for the inviscid flow, as has been proposed in Section 4.3.2 for the airplane;
- a 3D Navier–Stokes parabolic solver for the roof and sides; and
- embedded 3D Navier–Stokes solvers for the wakes of the car body, the wheels and the wing mirrors?

As compared with the airplane problem, the iterative interfacing will be somewhat more complex; and it is probable that more iterations will be needed before the interactions between the regions—elliptic-inviscid, parabolic-viscid, and elliptic-viscid—have procured mutually agreeable solutions of the interlinked equations. It is not *certain* that the final result of the simulation will be the same as that of a single fine-grid elliptic

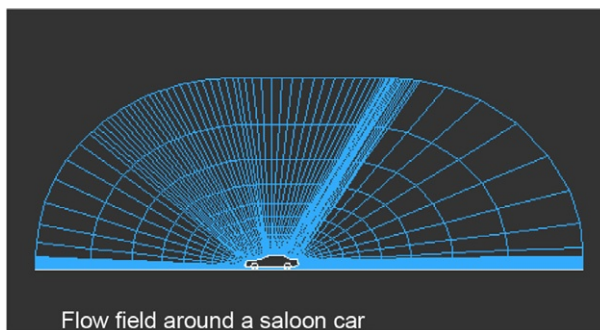


Figure 1.48 The whole grid.

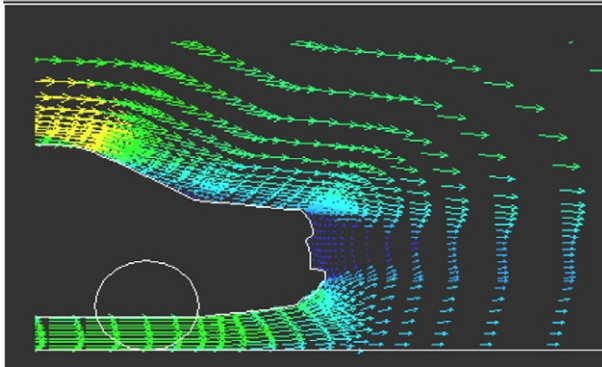


Figure 1.49 The wake.

Navier–Stokes solution for the whole space or that the total time-and-memory computer resource will be smaller. But, it seems highly probable and certainly worth a try.

4.3.4 Environmental applications

For the design of wind farms and the investigation of atmospheric-pollution phenomena, it is necessary to calculate the fields of velocity, temperature, and concentration in the atmospheric boundary layer, in spaces that extend several kilometers in the horizontal directions but have much smaller vertical heights. Such problems are well suited to solution by the partially parabolic method; although the wind directions are different near the ground at higher altitudes, the differences are not so great that a single direction of “marching integration” cannot be found for which all normal-to-plane velocities are negative. In other words, a “predominant direction of flow” can exist.

Probably no part of the domain can be regarded as inviscid; so the problem is more akin to the curved-duct and ship’s-stern problems, which were solved already in the 1970s. So much the better! Nevertheless, it would be possible to profit from the iteration-between-linked-regions technique that has been outlined in the foregoing [Sections 4.3.2 and 4.3.3](#). Finer-grid partially parabolic regions can be embedded inside coarser-grid ones, in the same way as elliptic regions.

Lastly, let flow over an urban terrain be considered, for example, the campus of the university of Delft, shown in [Fig. 1.50 \[56\]](#). It is customary to employ 3D elliptic solvers for simulating such flows, with the finest grid that can be afforded (1 m in the case illustrated).

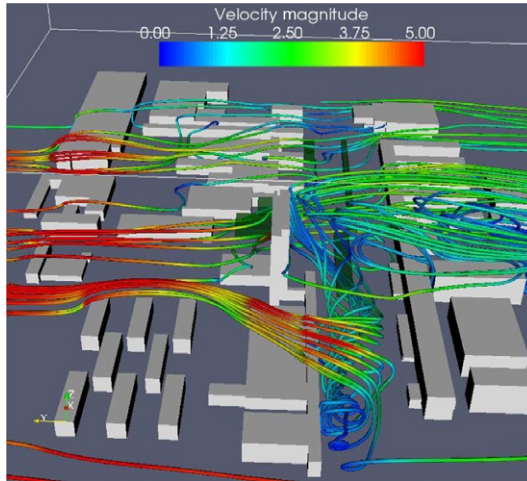


Figure 1.50 Urban-terrain simulation.

Inspection of the streamlines confirms the expectation that the prevailing wind enforces a predominant direction of flow in most of the space but that recirculation regions do exist in the wakes of the buildings. It follows that the original partially parabolic method *cannot* be used; but the extended one, which allows the embedding of recirculation regions as was outlined in connection with flow around cars, *can* be employed.

Of course, the number of recirculation regions may be rather large; but

- the flows within them need not be simulated simultaneously;
- visiting them in the order upstream-before-downstream will maximize speed of convergence;
- usually only a few of them are of interest to the user, so it makes sense to select them for most frequent and finest-grid treatment.

Generally speaking, the hybrid-CFD approach of the present “try-on” will allow, it is suggested, choices to be made that are optimal in respect to both economy and fitness for purpose.

4.3.5 Generalizing wall functions

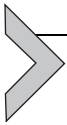
In natural- or urban-terrain simulations, it will often be useful to split the whole atmosphere into at least an upper and a lower region. The surface separating them, which might be either horizontal or parallel to the undulating ground, should be high enough to ensure that no flow occurs in the direction opposite to the predominant one. Then, the original partially parabolic

method can be used for the upper region; and any embedded elliptic volumes are contained within the lower one.

Of course, the two regions must exchange information, between iterations, regarding the pressures above and below the boundary and the fluxes of mass and of horizontal-direction momentum across it; and, as far as the upper region is concerned, this might as well be cast in wall-function form.

There is no need to go further; but far-seeing researchers might perceive that, once very many such situations have been analyzed, it may be possible to recognize quantitative connections between the aforesaid fluxes and some averaged properties of the below-dividing-surface contents. Thus, the effective shear-stress coefficient might be expected to depend on the amount of solid material, its surface area, and the typical solid-element size. One day indeed, a large-scale research program might be instituted of which the final deliverable would be a comprehensive set of properly parameterized formulas for the “effective roughness” of forests and cities. These could be used by practicing engineers, town planners, and environmentalists who had not time themselves to make massive CFD calculations.

Alas, no such pragmatic research programs are visible on the current scientific scene; but, when funding agencies are more wisely directed, they may appear in the future.



5. CONCLUDING REMARKS

The earlier-mentioned miscellany of fact and speculation, of history and prophesy, of argument and opinion, and of “broad-brush” and “nitty-gritty” has been launched with the motives expressed in the abstract. Readers who reach the end, will now look on CFD/CHT, it is hoped, as less daunting and awesome than they thought; and also as less *finished*. If some of them are caused to think “I believe that I could do better than *that*, the author will be well pleased.”

REFERENCES

- [1] A.K. Singhal, D.B. Spalding, Mathematical modelling of multiphase flow and heat transfer in steam generators, in: *Multiphase Transport: Fundamentals, Reactor Safety, Applications*, vols. 1–5, Hemisphere Publishing, Washington, DC, 1980, pp. 373–406.
- [2] C.S. Peskin, Flow patterns around heart valves: a digital computer method for solving the equations of motion, PhD thesis, Albert Einstein Coll. Med, 1972.
- [3] S. Kang, An improved immersed boundary method for computation of turbulent flows with heat transfer, PhD thesis, Stanford University, 2008.
- [4] L.S. Caretto, R.M. Curr, D.B. Spalding, Two numerical methods for three-dimensional boundary layers' computer methods, *Appl. Mech. Eng.* 1 (1) (1972) 39–57.

- [5] S.V. Patankar, D.B. Spalding, A calculation procedure for heat, mass & momentum transfer in three-dimensional parabolic flows, *Int. J. Heat Mass Transf.* 15 (1972) 1787–1806.
- [6] G.H. Golub, C.F. van Loan, *Matrix Computations*, fourth ed., John Hopkins, 2013.
- [7] Y. Saad, *Iterative Methods for Sparse Linear Systems*, SIAM Publications, Philadelphia, 2003.
- [8] M.R. Hestenes, E.L. Stiefel, Method of conjugate gradients for solving linear systems, *J. Res. Natl. Bur. Stand. B* 49 (1952) 409–436.
- [9] B.E. Launder, D.B. Spalding, *Mathematical Models of Turbulence*, Academic Press, London and New York, 1972.
- [10] J. Boussinesq, Theorie de l'écoulement turbulente, *Mem. Pre. Par. Div. Sav.* 23 (1877), Paris.
- [11] L. Prandtl, Bericht ueber Untersuchungen zur ausgebildeten Turbulenz, *ZAMM* 3 (1925) 136–139.
- [12] A.N. Kolmogorov, Equations of motion of an incompressible turbulent fluid, *Izv. Akad. Nauk. SSSR Ser. Phys. VI* (1–2) (1942) 56.
- [13] L. Prandtl, Ueber ein neues formelsystem fuer die ausgebildete turbulenz, *Nachr. Akad. Wiss. Goettingen* (1945).
- [14] F.H. Harlow, P.I. Nakayama, Turbulence transport equations, *Phys. Fluids* 10 (11) (1967) 2323–2332.
- [15] D.B. Spalding, *GENMIX: A General Computer Program for Two-Dimensional Parabolic Phenomena*, Pergamon Press, Oxford, 1977.
- [16] P.G. Saffinan, A model for inhomogeneous turbulent flow, *Proc. R. Soc. London A* 317 (1970) 417–433.
- [17] D.B. Spalding, The prediction of two-dimensional steady turbulent elliptic flows, in: *ICHMT Seminar, Herceg Novi, Yugoslavia, 1969*, See also D. Brian Spalding, A two-equation model of turbulence, *VDI Forschungsheft* 549 (1972) 5–16.
- [18] D.C. Wilcox, Multiscale model for turbulent flows, *AIAA J.* 26 (1988) 1311–1320.
- [19] S.V. Patankar, D. Brian Spalding, *Heat and Mass Transfer in Boundary Layers*, first ed., Intertext, London, 1967, 2nd ed. 1970.
- [20] A.D. Gosman, W.M. Pun, A.K. Runchal, D.B. Spalding, M. Wolfshtein, *Heat and Mass Transfer in Recirculating Flows*, Academic Press, London, 1969.
- [21] D.B. Spalding, A single formula for the law of the wall, *Trans. ASME E J. Appl. Mech.* 28 (1961) 455–458.
- [22] M.A. Leschziner, et al., (Ed.), *Proceedings of ETMM8, Marseille, France, 2010*.
- [23] U. Schuhmann, G. Groetzbach, L. Kleiser, Direct numerical simulation of turbulence, in: W. Kollmann (Ed.), *Prediction Methods for Turbulent Flows*, von Karman Institute, 1980.
- [24] W. Rodi, G. Constantinescu, T. Stoesser, *Large-Eddy Simulation in Hydraulics*, CRC Press, 2013.
- [25] D.B. Spalding, PPA's & PPB's, facilitating the comparison of experimental & DNS-, LES-, PANS-, PDF-transport and MFM models of turbulence, in: M.A. Leschziner, et al., (Ed.), *Proceedings of ETMM8, Marseille, France, 1, 2010*, p. 343.
- [26] D.B. Spalding, Turbulent mixing and chemical reaction; the multi-fluid approach. http://www.cham.co.uk/phoenics/d_polis/d_lecs/mfm/mfm00.htm, 1995–2010.
- [27] D.B. Spalding, Benjamin Franklin and computational fluid dynamics: the population approach to turbulence, *ASME J. Heat Transf. Comput. Fluid Dyn.* 0022-1481, 135 (2013) 011005-1–011005-12.
- [28] D.B. Spalding, Combustion and turbulence; old models and new, in: *Huw Edwards Award Lecture, Institute of Physics, 2012*.
- [29] D.B. Spalding, Mixing and chemical reaction in steady confined turbulent flame, in: *Proceedings 13th International Combustion Symposium, The Combustion Institute, 1971*, pp. 649–657.

- [30] D.B. Spalding, Numerical computation of multiphase flow and heat-transfer, in: C. Taylor, K. Morgan (Eds.), *Contribution to Recent Advances in Numerical Methods in Fluids*, Pineridge Press, Swansea, 1980, pp. 139–167.
- [31] PHOENICS Library Case W979. http://www.cham.co.uk/phoenics/d_polis/d_applic/d_react/2flrpl.htm.
- [32] D.B. Spalding, Models of turbulent combustion, in: *Proc. 2nd Colloquium on Process Simulation*, Helsinki University of Technology, Espoo, Finland, 1965, pp. 1–15.
- [33] G.C. Williams, H.C. Hottel, A.C. Scurlock, in: *Third Symposium on Combustion*, Williams and Wilkins, 1949, p. 21.
- [34] C. Dopazo, E.E. O'Brien, An approach to the auto-ignition of a turbulent mixture, *Acta Astronaut.* 1 (1974) 1239.
- [35] S.B. Pope, A Monte Carlo, Method for the PDF equations of turbulent reactive flow, *Combust. Sci. Technol.* 25 (1981) 150–174.
- [36] D.B. Spalding, Enlarging the frontiers of computational heat transfer, in: *Advances in Computational Heat Transfer*, CHT-8, Marrakech, 2008.
- [37] S.M. Klausmeyer, Comparative results from a CFD challenge over a 2D three-element high-lift airfoil, in: *NASA Technical Memorandum 112858*, 1997.
- [38] E.M. Sparrow, R.D. Cess, *Radiation Heat Transfer*, Wadsworth Inc., California, 1966.
- [39] S.G. Martyushev, M.A. Sheremet, Characteristics of Rosseland and P-1 approximations in modeling nonstationary conditions of convection–radiation heat transfer in an enclosure with a local energy source, *J. Eng. Thermophys.* 21 (2012) 111–118.
- [40] D.B. Spalding, Calculation of turbulent heat transfer in cluttered spaces, in: *Proc. 10th Int. Heat Transfer Conference*, Brighton, UK, 1994.
- [41] V.W. Nee, L.S.G. Kovasnay, The calculation of the incompressible turbulent boundary layer by a simple theory, in: *Proc. AFOSR/IFP Conference on Computation of Turbulent Boundary Layers*, 1968.
- [42] P.R. Spalart, S.R. Allmaras, A one-equation turbulence model for aerodynamic flows, *La Recherche Aérospatiale* 1 (1994) 5–21.
- [43] P.R. Spalart, Strategies for turbulence modelling and simulations, *Heat Fluid Flow* 21 (2000) 252–263.
- [44] S. Deck, P. Duveau, P. D'Espiney, P. Guillen, Development and application of Spalart–Allmaras one-equation turbulence model to three-dimensional supersonic complex configurations, *Aerosp. Sci. Technol.* 6 (2002) 171–183.
- [45] R. Gran Ollson, Geschwindigkeitsuns temperatur verteilung hinter einem gitter bei turbulenter stroemung, *ZAMM* 16 (1936) 257–267.
- [46] J. Nikuradze, Gesetzmaessigkeit der turbulenten Stroemung in glatten Rohren, *VDI Forschungsheft* 356 (1932) 20.
- [47] E.R. Van Driest, On turbulent flow near a wall, *J. Aerosp. Sci.* 23 (1956) 1007.
- [48] F.T.C. Thangam, C.G. Speziale, Turbulent separated flow past a backward-facing step; a critical evaluation of two-equation turbulence models, in: *NASA Contractor Report 187532 AD-A233 478*; ICASE Report No. 91-23, 1991.
- [49] J. Frohlich, D. von Terzi, E. Severac, R. Vaibar, Hybrid LES/RANS simulations—state of the art and perspectives, in: *Proceedings ETMM8*, Marseille, France, 2010.
- [50] V.S. Pratap, D.B. Spalding, Numerical computations of the flow in curved ducts, *Aeronaunt. Q.* 26 (1975) 219–228.
- [51] A.M. Abdelmeguid, N.C. Markatos, K. Muraoka, D.B. Spalding, A comparison between the parabolic and partially-parabolic solution procedures for three-dimensional turbulent flows around ships' hulls, *Appl. Math. Model.* 3 (4) (1979) 249–258.
- [52] A.K. Singhal, D.B. Spalding, A two-dimensional partially-parabolic procedure for axial-flow turbomachinery cascades, in: *Aero. Res. Council Report Number R&M 3807*, 1978.

-
- [53] R. Mittal, G. Iaccarino, Immersed boundary methods, *Annu. Rev. Fluid Mech.* 37 (2005) 239–261.
 - [54] http://www.cham.co.uk/phoenics/d_polis/d_enc/enc_rad3.htm.
 - [55] D.B. Spalding, in: *Lecture at Third International Symposium: Heat Transfer & Hydrodynamics in Swirling Flows*, Moscow Power Engineering Institute, 2008.
 - [56] S. Kenjeres, B. ter Kuile, Modelling and simulations of flow, turbulence and dispersion in urban environments with non-homogenous vegetation, in: *Proceedings of ETMM8*, Marseille, France, 2010, p. 170.
 - [57] D.B. Spalding, S.V. Zhubrin, X-cell: a new algorithm for fluid-flow simulation in PHOENICS, 1996, http://www.cham.co.uk/phoenics/d_polis/d_enc/x-cell.htm.
 - [58] http://www.cham.co.uk/phoenics/d_polis/d_enc/parsol.htm.
 - [59] http://www.cham.co.uk/phoenics/d_polis/d_applic/applic.htm.
 - [60] http://www.cham.co.uk/phoenics/d_polis/d_enc/x-cell.htm.